Ash Impacts on Gasoline Particulate Filter Performance and Service Life

by

Nicholas C. Custer

B.S. Naval Architecture and Marine Engineering
United States Coast Guard Academy, 2009

Submitted to the Department of Mechanical Engineering in Partial Fulfillment of the Requirements for the Degrees of

MASTER OF SCIENCE IN MECHANICAL ENGINEERING
AND
MASTER OF SCIENCE IN NAVAL ARCHITECTURE AND MARINE ENGINEERING

AT THE

MASSACHUSETTS INSTITUTE OF TECHNOLOGY

June 2015

Signature of Author: Signature redacted
Department of Mechanical Engineering
May 8, 2015

Certified by: Signature redacted
Victor W. Wong
Principal Research Scientist and Lecturer in Mechanical Engineering
Thesis Supervisor

Accepted by: Signature redacted
David Hardt
Chairman, Department Committee on Graduate Students

(This page intentionally left blank)

Ash Impacts on Gasoline Particulate Filter Performance and Service Life

by

Nicholas C. Custer

Submitted to the Department of Mechanical Engineering on May 8, 2015 in Partial Fulfillment of the Requirements for the Degree of

MASTER OF SCIENCE IN MECHANICAL ENGINEERING
AND
MASTER OF SCIENCE IN NAVAL ARCHITECTURE AND MARINE ENGINEERING

ABSTRACT

New regulations in the United States and Europe, designed to address climate change concerns by reducing greenhouse gas emissions, are causing increased use of gasoline direct-injection (GDI) engines in light-duty vehicles (LDV). Separate new regulations that aim to reduce particulate emissions to address air pollution concerns are taking effect concurrent with greenhouse gas limitations in both jurisdictions. GDI engines are proven to create more particulate emissions than previously utilized port-injection technology. Increasing particulate emissions rates combined with falling regulatory particulate emissions limits requires new strategies to reduce these emissions from gasoline powered LDVs.

Particulate filters have been successfully implemented to reduce particulate emissions from diesel engine exhaust for over a decade. Diesel particulate filters have a demonstrated filtration efficiency of 95% or greater and have reduced diesel particulate mass (PM) emissions by one to two orders of magnitude. GDI engines require no more than one order of magnitude reduction in particulate emissions to meet new regulations. Existing particulate filter technology in use in diesel vehicles is capable of reducing GDI engine emissions to new regulatory levels; however, it is proposed that these reduction may be achievable through means other than gasoline particulate filters (GPF).

A GPF will create an additional backpressure in the engine exhaust system that will reduce engine power and efficiency. This backpressure will increase as PM is trapped in the filter and decrease as combustible PM removed. A buildup of incombustible ash present in engine-out PM will increase the baseline backpressure of the filter during the course of its service life. It is important to understand the impact of ash on the filter pressure drop performance before implementing GPF to meet new emissions regulations.

This study builds on existing diesel particulate filter technology and demonstrates through experimental results the mechanisms by which ash increases GPF pressure drop. Ash deposits are also shown to increase the light-off temperature of three-way catalyst coatings in GPF.

Thesis Supervisor: Victor W. Wong
Title: Principal Research Scientist and Lecturer in Mechanical Engineering

(This page intentionally left blank)

Acknowledgments

I have hoped for an opportunity to study at MIT since my times as an undergraduate at the Coast Guard Academy. It was there that I developed my love of engineering and at the same time learned about the impressive opportunities available to graduate students at MIT. I would like to thank Dr. Todd Taylor, CAPT John Reeves, LCDR Nicholas Parker, CDR Michael Corl and Dr. Kurt Colella, among many others, for guiding me through the formative years of my engineering education and setting me on the path to where I am today.

My time at MIT has been extremely challenging and rewarding. First and foremost I would like to thank my thesis advisor, Dr. Victor Wong, for giving me the opportunity to work at the Sloan Automotive Engine Laboratory and supporting me throughout my time at MIT in every way imaginable. Dr. Wong's advice and wisdom throughout my research at the Sloan lab moved my research forward and his flexibility and positive foresight allowed me to reach all of my goals during two years as a master's student.

My research project would not have been possible without the support of the Ford Motor Company. I would like to thank James Pakko, Christine Lambert, Christoph Boerensen, and Tim Chanko for all of their advice, guidance, and patience throughout this project. I have learned a lot about conducting research and the realities of engineering outside of an academic setting from our interactions.

I would like to thank Dr. Carl Justin Kamp for his continuous encouragement, guidance, and support on this project. I doubt that I will again encounter someone with the impressive combination of scientific knowledge, curiosity, and work ethic that Dr. Kamp brings to the lab every day. I could not have reached my research goals without the mountain of effort that he has contributed to this project. Thank you also to Dr. Alexander Sappok for the invaluable wisdom and guidance on this project.

My research would not have been possible without the help of the highly skilled and professional staff at the automotive engine lab. Thank you to Thane DeWitt, Raymond Phan, and Janet Maslow for the constant and unwavering support.

To my lab mates, Tim Murray, Paul Folino, James Jorgensen, Greg Monahan, and Michael Arnold, thank you for all of the advice, both academic and otherwise. Time spent in the office covered the spectrum of productivity but was crucial to answering the tough questions as research progressed and maintaining balanced mental health over two long years.

I would like to thank the US Coast Guard allowing me the opportunity to spend two years as a full time student in the midst of my career. Thank you also to the US Navy 2N program for supporting me during my time at MIT and facilitating my continued study of Naval Architecture.

Finally, I would like to thank my loving family for supporting and encouraging me all along the way. My time at MIT represents the culmination of a long academic career made possible by the massive influence of a family full of teachers showing me how to push myself to succeed in all endeavors. Thank you for the love and sacrifices that led me to this point.

(This page intentionally left blank)

Table of Contents

List of Figures

(This Page Intentionally Left Blank)

List of Tables

(This page intentionally left blank)

List of Abbreviations

AFR – Air to Fuel Ratio by Mass
AFR_S – Stoichiometric Air to Fuel Ratio
C-GPF – Catalyzed GPF
CO – Carbon Monoxide
CO_2 – Carbon Dioxide
DPF – Diesel Particulate Filter
ECM – Engine Control Module
EPA – Environmental Protection Agency
FTIR – Fourier Transform Infrared Spectroscopy
GDI – Gasoline Direct Injection
GHG – Greenhouse Gas
GPF – Gasoline Particulate Filter
GPI – Gasoline Port Injection
GTDI – Gasoline Turbocharged Direct Injection
HC – Hydrocarbon
H/C – Fuel Hydrogen to Carbon Ratio
H_2O – Water
LDV – Light-Duty Vehicle
MY – Model Year
NHTSA – National Highway Traffic Safety Administration
NMOG – Non-Methane Organic Masses
NO – Nitric Oxide
NO_2 – Nitrogen Dioxide
NO_X – Nitrogen Oxides
PM – Particulate Mass
PN – Particulate Number
SI – Spark Ignition
SOF – Soluble Organic Fraction
TWC – Three Way Catalyst
VOC – Volatile Organic Compounds
γ – Heat Capacity Ratio
$\eta_{f,i}$ – Thermodynamic Efficiency

(This Page Intentionally Left Blank)

1. Introduction

The transportation sector consumes 28% of total energy usage in the United States and contributes 27% of US greenhouse gas (GHG) emissions [1, 2]. Vehicles powered by gasoline internal combustion engines consume 57% of US transportation energy [1]. Reducing GHG emissions has become an important part of curbing global climate change. In April 2010, the US Environmental Protection Agency (EPA) and National Highway Traffic Safety Administration (NHTSA) established final rules for phase one on the Light-Duty Vehicle (LDV) Greenhouse Gas Emissions and Corporate Average Fuel Economy Standards (CAFE) setting goals to reduce fleet wide CO_2 emissions and increase fleet average fuel economy [3]. The final rule for phase two of this effort was passed in October 2012. CAFE standards aim to reduce the fleet average CO_2 emissions for LDVs by 45% between model year (MY) 2012 and MY2025 with an associated increase in fleet average fuel efficiency of 81% [3, 4].

To address vehicle emissions other than GHG, the EPA will implement Tier 3 Motor Vehicle and Fuel Standards in 2017. This regulation will set strict limits on vehicle tailpipe emissions of non-methane organic gasses (NMOG), nitrogen oxides (NO_X), and particulate mass (PM). Tier 3 standards aim to reduce NMOG+NO_X emissions levels by 70% and PM emissions by 80% relative to current fleet averages. These standards will phase in from MY2017 to MY2025 concurrent with the phase in of CAFE standards. The final Tier 3 PM emissions limit for LDV is 3mg/mi [5].

For the European market, Euro 6 emissions standards were adopted in 2007. Euro 6 includes a PM limit for gasoline direct injection (GDI) engines of 4.5 mg/km (7.2mg/mi) but also includes an additional limitation on particle number (PN) emissions of $6.0x10^{11}$ particles/km. This requirement will phase in for GDI engines with an initial standard of $6.0x10^{12}$ particles/km taking force this year and the full Euro 6b limit of $6.0x10^{11}$ particles/km beginning in 2018 [6]. Analysis of diesel soot has estimated that there are approximately $2.0x10^{12}$ particles per mg of soot [7]. Utilizing this value for a first order estimate of GDI soot emissions, the PM level equivalent to the Euro 6b PN limit of $6.0x10^{11}$ particles/km is 0.3mg/km (0.48mg/mi). This limit is an order of magnitude lower than the PM limits set by Tier 3 and Euro 6 for GDI engines. Emissions levels for current GDI engine technology also show that the Euro 6b PN limit requires

the largest particulate emission reduction relative to current levels. Current technology can perform near Tier 3 and Euro 6 PM limits but are an order of magnitude above the Euro 6b PN limit [8].

1.1 Increased Use of Gasoline Direct-Injection

One strategy for fleet-wide fuel economy improvement for gasoline engines to meet CAFE standards is implementation of GDI engines. Direct injection offers improvements in an engine's thermal efficiency over gasoline port injected (GPI) engines because the latent heat of vaporization of the liquid fuel is drawn from the charge air for GDI. In GPI engines the vaporization energy is predominantly drawn from solid surfaces in the air intake manifold such as the manifold walls and intake valve. In cylinder vaporization of the fuel spray in a GDI engine increases the heat capacity ratio (γ) of the charge mixture. Higher γ increases the thermodynamic efficiency ($\eta_{f,i}$) of the engine cycle, which is given in equation 1 [9, 10].

$$\eta_{f,i} = 1 - \frac{1}{r_c^{\gamma-1}} \tag{1}$$

GDI can also pair well with engine downsizing and turbo charging to further increase fuel efficiency to meet CAFE standards [9]. Reducing the engine displacement will increase the overall fuel efficiency by forcing the engine to operate at higher load levels during normal operation. The engine is then turbocharged to increase the volumetric efficiency in order to achieve the required peak power with smaller displacement. A drawback of this strategy is that the resulting downsized turbocharged engine will operate at a higher compression ratio and therefore be more prone to knocking during high load operation. Direct-injection of the fuel to the cylinder is an effective knock mitigation strategy for this type of engine. The result is a gasoline turbocharged direct injection (GTDI) engine with higher fuel efficiency and a smaller displacement than a naturally aspirated port-injected engine of similar power.

GDI mitigates engine knock by reducing the charge temperature when compared with GPI by changing the source of the latent heat of vaporization. In the case of GDI the majority of the latent heat is taken from the charge air. For GPI the latent heat is primarily conducted from the

surfaces of the inlet manifold and intake valve, cooling those solid components and not the charge gases. The reduction in charge temperature with GDI maintains the end gas pressure below the knock limit at higher compression ratios resulting in higher volumetric and thermodynamic efficiency for the GTDI engine at peak power. The EPA and NHTSA project market penetration of 94% for GDI and 89% for turbocharged-downsizing by MY2025 [9]. With the increase usage of this technology comes two notable disadvantages, increased cost and increased particulate emissions.

The component cost of direct-injection fuel systems is higher than port-injection fuel systems primarily because of the pressures required for the atomizing fuel spray needed to facilitate in-cylinder fuel vaporization. The normal fuel pressure for GPI is 3-7bar resulting in fuel droplets of 80-200μm [11]. Direct-injection requires smaller fuel droplets to promote vaporization in the charge gases without the help of hot surfaces that facilitate evaporation for port-injection. The fuel pressure for GDI is 50-150bar to produce fuel droplets of 15-50μm [11]. The direct-injection fuel system requires a high-pressure fuel pump and nozzles that can handle these pressures. Direct-injection nozzles also require higher cost materials and manufacturing to operate in a harsher in-cylinder environment compared with port-injection nozzles located in the inlet manifold. The one time added cost of direct-injection systems has discouraged their use in spark ignition engines in the past. However the need to implement fuel economy improvements to meet CAFE standards combined with the increasing cost benefit of fuel economy with rising gasoline prices makes direct-injection fuel systems a critical part of future LDV engine design.

1.2 Combustion and Stoichiometry

Chemical energy is converted to thermal energy inside a gasoline engine through combustion. The thermal energy is then converted to mechanical energy and output as mechanical work. During ideal combustion an oxidizer reacts with hydrocarbon species to form CO_2 and H_2O. Actual engine combustion does not result in full oxidation of all fuel hydrocarbons resulting in secondary products in addition to CO_2 and H_2O. In consumer vehicles the oxidizer for the combustion reaction is oxygen present in atmospheric air. Additional oxidizers may be introduced in some unique applications.

Gasoline can consists of over 200 different hydrocarbon species. Each species will have its own stoichiometric balance for ideal combustion. The average hydrogen to carbon (H/C) ratio of gasoline is 1.87 and the molecular weight is ~110[10]. Iso-octane is a useful substitute for gasoline with a H/C ratio of 2.25 and molecular weight of 114. The balanced stoichiometric combustion reaction for Iso-octane reacting with air is given in equation 2.

$$C_8H_{18} + 12.5(O_2 + 3.773N_2) \rightarrow 8CO_2 + 9H_2O + (12.5 * 3.773)N_2 \quad (2)$$

The molar ratio of air to iso-octane for ideal stoichiometric combustion is 12.5. The stoichiometric air to fuel ratio by mass is found by applying the molecular weights of iso-octane and air to the molar ratio. The stoichiometric air to fuel ratio (AFR_S) for iso-octane is 15.13[10]. Calculation of AFR_S for gasoline is complicated by the number of unique hydrocarbon species present but has been found to be 14.6 [10].

The air fuel ratio (AFR) in a spark ignition (SI) engine must be maintained as close to AFR_S as possible to maximize efficiency and power output, and to ensure proper operation of the three-way catalyst (TWC) to limit vehicle emissions. At AFR_S all fuel will be fully oxidized with no excess oxygen remaining. Full oxidation of the hydrocarbon fuel minimizes specific fuel consumption, maximizing efficiency. Consumption of all oxygen present maximizes power output for a given cycle because the largest possible fuel charge is combusted. Figure 1-1 shows the composition of dry exhaust gases from a SI engine as a function of AFR. In this plot AFR is represented by the Equivalence Ratio (Φ) described in equation 3.

$$\Phi = \frac{AFR}{AFR_S} \quad (3)$$

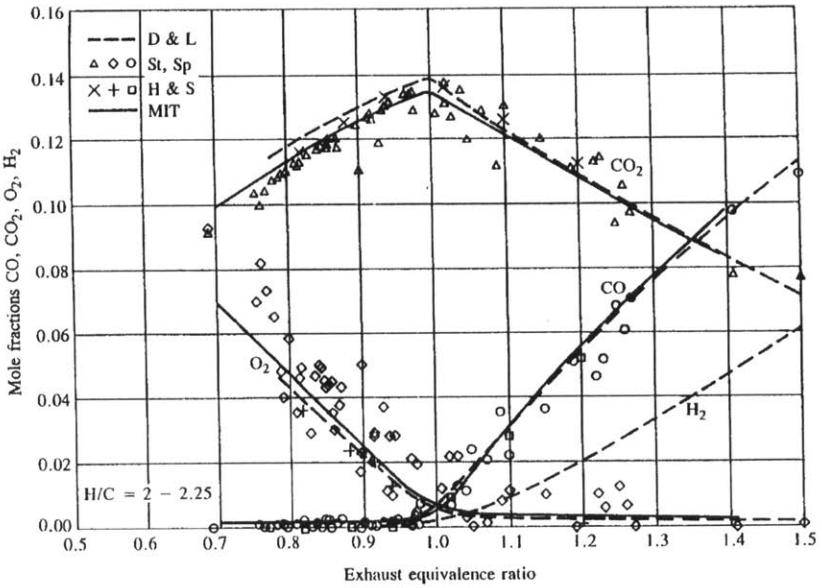

Figure 1-1 – Internal Combustion Engine Major Exhaust Constituents as a Function of Equivalence Ratio [10]

Independent of fuel efficiency and power output, the overall AFR for a modern SI engine must be maintained at AFR_S to facilitate proper operation of the exhaust catalyst. Commonly referred to as the catalytic converter, the exhaust catalyst is responsible for removing harmful combustion products from a vehicle's exhaust stream prior to emission from the tailpipe. Modern three-way catalysts require stoichiometric engine exhaust in order to function properly. The TWC will be discussed further in section 1.3.6.

1.3 Engine Emissions and Emissions Controls

The primary products of hydrocarbon oxidation were outlined in section 1.2 and are shown in Figure 1-1. Several additional chemical and physical processes occur inside the engine cylinder and exhaust manifold that lead to additional engine out exhaust constituents. Several of these additional constituents along with carbon monoxide present significant health and environmental hazards. Regulations limiting these pollutants are in place and reduction strategies including the TWC are in use to limit their release into the atmosphere. It is important to understand the formation mechanism of these pollutants, their health effects, and the strategies to reduce them through engine exhaust gas after treatment before considering new after treatment technology.

1.3.1 Nitrogen Oxides

A large amount of diatomic nitrogen is present in the engine cylinder because it is drawn in from the atmosphere with the oxygen needed for combustion. Formation of NO follows the extended Zeldovich mechanism, which consists of three separate chemical reactions represented in equations 4, 5, and 6 [10].

$$O + N_2 \rightarrow NO + N \quad (4)$$

$$N + O_2 \rightarrow NO + O \quad (5)$$

$$N + OH \rightarrow NO + H \quad (6)$$

Combustion generates a small number of independent oxygen atoms that are capable of reacting with a normally stable diatomic nitrogen molecule at temperatures greater than 2000K to form nitric oxide (NO) [10]. The resulting nitrogen atom is highly reactive and will quickly react with either oxygen or hydroxide to form a second NO molecule. The reaction given in equation (4) is the rate-limiting step of this mechanism. NO formation continues after combustion until the exhaust stream cools below 2000K at which point NO concentrations are frozen. Some NO molecules are further oxidized to NO_2 in the combustion chamber. The resulting mixture of nitrogen oxides is commonly referred to as NO_x. NO_2 can constitute 10-30% of total NO_x in compression ignition engine exhaust. However, the NO_2 fraction of NO_x in an SI engine is normally negligible and makes-up at most 2% of total NO_x. The NO_x concentration in engine out exhaust for an SI engine ranges from 500-2000ppm [10].

NO_x emissions contribute to air pollution by elevating levels of ozone and NO_2 in the lower atmosphere. NO_x emitted from the vehicle tailpipe is almost entirely NO. The NO emitted from the vehicle will react with volatile organic compounds (VOC) (also emitted from vehicles and discussed in section 1.3.2) in the presence of sunlight to form ozone through the photochemical smog formation process. A series of complex reactions will continuously generate and break down ozone in the atmosphere but with sufficient sunlight, atmospheric temperatures, and supply of NO and VOCs, ozone levels will rise [9]. NO_2 is also generated during the balanced reactions of NO and ozone. Both ozone and NO_2 are harmful air pollutants that have been shown to

contribute to asthma attacks, pulmonary inflammation, and respiratory irritation particularly in children, elderly adults, and individuals with respiratory diseases [12, 13].

1.3.2 Unburned Hydrocarbons

The hydrocarbon fuel introduced into the engine cylinder will not be fully oxidized during the combustion process. There are four processes that can generate unburned hydrocarbons (HC) in a typical SI engine. Flame quenching at cool surfaces on the cylinder walls can leave a thin layer of unburned mixture after combustion. Portions of the unburned mixture can enter crevice areas in the cylinder and escape combustion when flame quenching occurs at the crevice entrance. HC can absorb into lubricant oil films on the cylinder walls prior to ignition and desorb into the burned gases after combustion. Large quantities of HC can be generated by cylinder misfires or incomplete combustion of the charge, which can occur during cold start or major engine transients when gas temperature, air fuel ratio, spark timing, and exhaust gas recirculation are not ideal for combustion [10]. In addition to these mechanisms, fuel impingement on cylinder surfaces can generate HC emissions in a GDI engine.

Flame quenching occurs when the pre-mixed flame propagates near the cylinder walls or reaches a narrow crevice entrance. The engine coolant cools the cylinder walls and heat transfer from the end gas to the walls overcomes the heat release of the combustion leaving a layer of unburned or partially burned hydrocarbons along the quenching surface. In the case of crevice entrances, the increase in surface area to volume ratio elevates heat transfer and can quench the flame even if all surfaces are not cooled to the temperature of the cylinder walls. Typical quench layer thickness for an SI engine ranges from 0.05 to 0.4mm [10].

Crevices contribute a major portion of the total HC. There are several typical crevice areas in a SI engine cylinder, but the largest source of HC comes from the piston top land clearance crevice. This crevice is bounded by the cylinder wall, piston top land, and piston top ring. The cylinder walls cool this crevice charge resulting in a higher density than the bulk cylinder end gasses. As cylinder pressure rises during combustion, the total mass in the crevice increases. When the flame reaches the crevice entrance it quenches leaving unburned mixture in the crevice

volume. During the expansion stroke the crevice gasses expand and flow out of the crevice carrying HC into the burned gas mixture [10].

Incomplete combustion of the cylinder charge results in exhaust of the remaining stoichiometric mixture. In the case of misfire, the entire fuel mass injected during that cycle will contribute to unburned hydrocarbon emissions. This mechanism can create the largest volume of HC per cycle, but it does not occur regularly. Incomplete combustion occurs when the end gas temperature and pressure drop quickly enough during the expansion stroke to quench the flame in the bulk gas. This phenomenon can occur during light loading and engine transients. Improper spark timing, exhaust gas recirculation levels, and air fuel ratio are causative factors in incomplete combustion [10].

HC can enter the burned gas mixture by desorbing from the cylinder wall oil film after combustion. The hydrocarbons enter the cylinder as part of a stoichiometric mixture and begin to absorb into the oil film present on the cylinder wall and piston crown. As the mixture pressure increases during the compression stroke, the vapor pressure of hydrocarbons rises forcing further absorption of fuel vapors into the oil films. After combustion the partial pressure of hydrocarbons in the burned gas mixture is near zero, which drives desorption of the hydrocarbon species present in the oil film. This source of hydrocarbons is unique compared to flame quenching, crevice volumes, and incomplete combustion as a source of HC because the resulting hydrocarbons are no accompanied by unburned oxygen present in the original stoichiometric mixture levels [10].

Liquid fuel on the piston crown and cylinder surfaces in GDI engines is a fifth source of unburned hydrocarbon emissions for this engine type. When fuel is injected directly into the combustion cylinder, the fuel spray will impinge on the piston crown and cylinder walls. The location and degree of surface impingement depends on the injector type, location, and fuel spray aiming. For typical direct injection the largest fuel films will occur on the piston crown due to fuel spray impingement when the piston approaches top dead center. The resulting liquid fuel film or pools will not fully vaporize leaving liquid fuel present after combustion. A portion of these films will vaporize into the hot burned gasses after combustion contributing to hydrocarbon

emissions. The liquid fuel pools are also consumed by diffusion flame pool fires, which will be discussed in section 1.3.5. Pool fires limit the total mass of fuel that will vaporize into the burned gas mixture as HC. For optimum injection timing, the fuel film mass is sufficiently small that this source will contribute less than 15% of total HC. For sub-optimal injection timing fuel films from fuel spray impingement can contribute to higher hydrocarbon emissions but will never constitute more than 35% of the total HC from all sources [14].

The five source of hydrocarbons discussed above contribute to HC content in the burned gas mixture following combustion. Three of these mechanisms also contribute oxygen to the mixture. When HC and remaining oxygen mix with the hot burned gasses additional hydrocarbon oxidation will occur. Hydrocarbon oxidation continues during the exhaust process both in cylinder and in the hot exhaust manifold. In cylinder oxidation primarily impacts wall quench layer hydrocarbons. These species are in close proximity to hot burned gasses and oxygen and will oxidize readily. Other hydrocarbons will experience a majority of oxidation late in the exhaust stroke and in the exhaust manifold because they rely on longer residence times for mass transfer from crevices and mixing with available oxygen. As much as 50% of the HC present can be oxidized in cylinder and up to 40% of the remaining HC can be oxidized in the exhaust manifold [10].

These oxidation processes can produce CO_2 and H_2O, but partial oxidation is common generating CO and partially oxidized hydrocarbons as products. Pyrolysis also occurs at this stage generating soot from some unburned hydrocarbons. Pyrolysis is discussed in section 1.3.4 [10].

Hydrocarbons present multiple health risks. Many hydrocarbon species are highly reactive with NO to form NO_2. These species, referred to as VOCs, are a key reactant in the photochemical smog formation process and contribute to the negative health effects described in section 1.3.1 [9, 10]. In addition, certain hydrocarbon species are known carcinogens. Benzene is one example that has been shown to cause leukemia by all routes of exposure. Benzene has also been linked to non-cancerous blood disorders and other negative health effects [9].

1.3.3 Carbon Monoxide

Carbon monoxide (CO) is generated during fuel combustion when incomplete oxidation of the hydrocarbon fuel occurs. The oxidation reactions necessary to breakdown large hydrocarbon species are complex. CO is one major product of the intermediate steps of the combustion reaction. After CO is produced in the combustion flame zone it is oxidized to form CO_2 to complete the ideal combustion reaction. In the cylinder during combustion these chemical reactions proceed at rates sufficient to maintain equilibrium between the products and reactants meaning that CO is present at the expected equilibrium level for the given temperatures and pressures. After combustion, the reaction remains in equilibrium as the charge cools during expansion, but after exhaust valve opening the rate of charge cooling increases and the chemical reactions of CO become kinetically limited and can no longer equilibrate. CO concentrations are effectively frozen at equilibrium values for temperature and pressure significantly above the eventual tailpipe out conditions [10].

Exposure to CO has been linked with several negative health effects. The EPA found that a casual link is likely between short term CO exposure and increased risk of cardiovascular disease. Other possible negative health effects include birth defects, preterm birth, and respiratory disease. Current evidence based on human epidemiology and animal toxicology suggests that both short term and long term CO exposure may contribute to these conditions [9, 15].

1.3.4 Particulate Emissions

Particulate mass (PM) in the engine exhaust stream is made-up of elemental carbon, incombustible ash derived from lubricant oil additives and engine wear particles, and soluble organic fraction (SOF) [16]. Elemental carbon particles, commonly referred to as soot, are the primary constituent of engine out PM. Soot forms in cylinder from fuel hydrocarbons when they are exposed to temperatures greater than $400^{O}C$ in the absence of oxygen. Under these conditions hydrocarbons decompose through pyrolysis to form soot precursor compounds that will react to form polycyclic aromatic hydrocarbon (PAH) molecules that in turn form soot [16].

Conditions required for soot formation can occur by two main mechanisms. Regions of very fuel rich mixture will combust leaving large concentrations of unburned hydrocarbons in an oxygen-depleted region. Soot formation will proceed as long as sufficient temperatures are maintained. Soot will also form through burning of a diffusion flame. In a diffusion flame, fuel vapors from a region of pure fuel in liquid and/or vapor form mix with air in the flame zone to form the reactants needed for the combustion reaction. The presence of pure fuel vapors adjacent to the flame zone creates ideal conditions for soot formation [16].

After the formation of soot precursors through partial oxidation and pyrolysis of larger hydrocarbons, soot will either oxidize in the cylinder or exhaust manifold or agglomerate and leave the engine as PM emissions. Soot precursors consist of a series of small hydrocarbon compounds that are easily oxidized prior to agglomeration. Precursors that come in contact with oxygen in the cylinder or exhaust manifold will likely oxidize and leave the engine as CO, CO_2, H_2O, and other secondary combustion products. Soot precursors that do not contact free oxygen will begin to nucleate with other precursors to form soot particles [8]. There are two modes of growth for soot particles after nucleation, surface growth and coagulation. Surface growth occurs when additional soot precursors meet and join existing soot particles. Surface growth leads to an increase in PM mass and mean particle size while PN remains constant. Coagulation occurs when two soot particles meet and combine to form a single larger particle. Mean particle size increases, PN decreases, and PM mass remains constant when coagulation takes place [8].

Short-term exposure to airborne particulates increases the risk of cardiovascular and respiratory illness including congestive heart failure, exacerbation of asthma, and respiratory infections. Long-term exposure to airborne particulates is associated with development of cardiovascular disease and respiratory effects including development of asthma and reduced lung function growth [9, 17]

1.3.5 Increased Particulate Emissions from Direct-Injection Engines

A homogeneous stoichiometric mixture of gasoline and air will not normally generate the conditions required for soot formation. GPI engines provide a well mixed near-homogenous charge that produces very little soot. In fact, GPI engines produce sufficiently low particulate

emissions that they are excluded from PM and PN regulation under Euro 6 rules [6]. GDI engines produce increased particulate emissions due to reduced mixing efficiency and increased fuel impingement on cylinder surfaces. Locally rich mixture pockets and liquid fuel droplets and pools provide the conditions needed for soot formation. Figure 1-2 demonstrates the sources of soot in GDI engines.

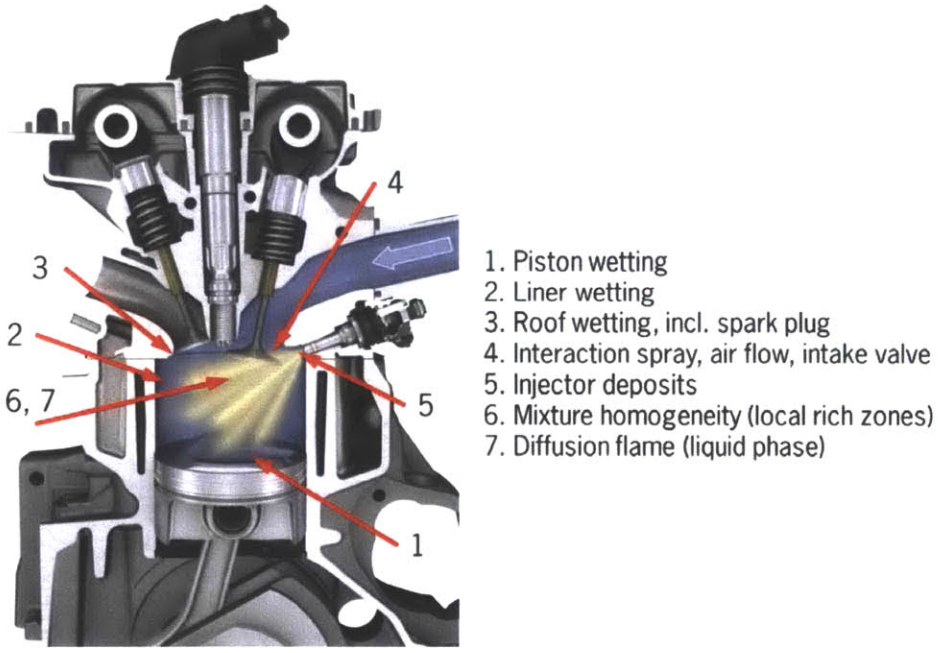

Figure 1-2 – Soot Sources in a GDI Engine [8]

Direct injection engines have an increased occurrence of locally rich pockets within the cylinder charge. First generation GDI engines utilized stratified charge combustion strategies that required injection during the compression stroke and deliberately generated a fuel rich region near the spark plug. These factors combined to promote increased soot formation compared to GPI engines in use at the time [8]. Current homogenous charge GDI engines maximize charge mixing by injecting during the intake stroke. The fuel air mixture is exposed to the period of highest charge motion and the mixing time is maximized [18]. Implementation of homogenous charge and reductions in cylinder component wetting has reduced both PM and PN emissions by an order of magnitude compared with first generation GDI engine technology [8].

Liquid fuel in the cylinder during combustion leads to diffusion flames that generate soot. GDI suffers from significant fuel impingement on cylinder walls and piston crown. Liquid fuel films

that result from fuel impingement on these surfaces cannot be fully consumed during the primary combustion event. Diffusion flame pool fires will persist from these areas of liquid fuel well after the main combustion is complete. The diffusion flames generate large amounts of soot that account for much of the additional particulate emissions generated by GDI engines compared with GPI engines [14]. Reductions in PM and PN emissions from 1st generation GDI to current technology are significant but current emissions fall near Tier 3 and Euro 6 PM limits and above the Euro 6 PN limit [8].

1.3.6 Three-way Catalyst

Current gasoline SI engine exhaust treatment is accomplished by the three-way catalyst (TWC), commonly referred to as the catalytic converter. The TWC's purpose is to remove NO_x, HC, and CO from the engine out exhaust stream through catalyzed chemical reactions before the exhaust exits the vehicle tailpipe and enters the atmosphere. The catalyst substrate is an extruded ceramic honeycomb with open channels along the flow axis. Figure 1-3 shows the typical geometry of the TWC substrate.

Figure 1-3 – Flow Through Ceramic Catalyst Substrate [19]

The ceramic honeycomb walls are coated with alumina (Al_2O_3), which acts as a high surface area carrier and support for catalyst particles in the TWC. Precious metal catalyst particles are deposited in the TWC on the surface of the alumina support to promote chemical oxidation of CO and HC and reduction of NO. Platinum particles are present to promote oxidation of CO to

CO_2 and HC to CO_2 and H_2O. Rhodium particles are present to promote reduction of NO. There are a series of possible reactions that will remove NO in a reducing atmosphere through reactions with CO or H_2 [10].

For catalyzed oxidation and reduction reactions to occur simultaneously in the TWC, the AFR of the engine must be maintained near stoichiometric within very small tolerances. Maintaining stoichiometric conditions will maintain proper concentrations of oxygen and reducing gases to allow the three desired reactions to proceed. The AFR tolerance of the TWC is not reasonably achievable during operation of a vehicle engine so designers employ a modulation strategy to maintain a suitable chemical environment in the TWC. The onboard electronic engine control module (ECM) will continuously monitor the exhaust for the presence of oxygen while modulating the AFR around AFR_s. A binary oxygen sensor provides feedback on the time span spent above and below AFR_s, which the ECM uses to adjust the mean value of the fuel flow modulation. This strategy results in alternating short periods of slightly fuel rich and slightly fuel lean operation. To maintain a suitable oxidizing and reducing environment continuously in the TWC, formulators add an oxygen storage catalyst [10].

Cerium is the primary oxygen storage catalyst utilized in the TWC. The storage catalyst will oxidize under fuel lean exhaust conditions to absorb excess oxygen from the exhaust stream and form cerium oxide (Ce_XO_Y) [10]. The absorption lowers oxygen levels allowing reduction reactions to proceed. During fuel rich engine operation cerium oxide is reduced in the TWC releasing oxygen molecules needed to continue oxidation of CO and HC. The presence of the oxygen storage catalyst combined with air fuel ratio modulation allows the TWC to continuously remove NO, CO, and HC from the exhaust stream with efficiency greater than 95% [11].

1.3.7 Diesel Particulate Filter

Combustion in a diesel engine predominantly involves a diffusion flame originating from a high-pressure direct fuel injection during combustion. The diffusion flame produces large amounts of soot causing high particulate emissions from diesel engines. Emissions regulations in the United States have required use of diesel particulate filters (DPF) for all medium and heavy duty on-road diesel vehicles since in 2007 [20]. Diesel particulate filters capture PM from the exhaust

stream and have been very successful in reducing tailpipe PM emissions from diesel vehicles with soot filtration efficiencies greater than 95% [20]. After PM is trapped in the filter, the soot and SOF portion are removed by oxidation that converts the PM to stable gaseous compounds. In the case of carbon soot the product in CO_2. This process is referred to as regeneration. The incombustible ash constituents of the trapped PM are not removed during regeneration and remain in the filter until they are physically removed through various methods of filter cleaning.

A DPF is the largest source of backpressure in a diesel engine exhaust system due to the flow resistance of the filtration mechanism in the filter. A clean DPF will create a significant pressure drop across it before any PM is captured. As PM is captured in the filter the pressure drop will increase by up to five times the original level as PM deposits reduce the porosity of the filter in turn reducing the permeability and increasing flow resistance [20]. A portion of this pressure drop increase is recovered when soot particles are removed through regeneration. However, incombustible ash deposits result in a permanent increase in the DPF pressure drop. The pressure drop across the DPF increases the engine exhaust pressure reducing engine power output and fuel efficiency. Power and efficiency losses increase as the filter ages and incombustible ash deposits grow. Typical pressure drop curves for several DPFs are shown in Figure 1-4. Pressure drop is plotted versus ash mass concentration in the filter given in grams of ash per liter of filter volume. These pressure drop measurements are taken with zero soot present in the DPF and represent the permanent increase in the DPF pressure drop during its service life.

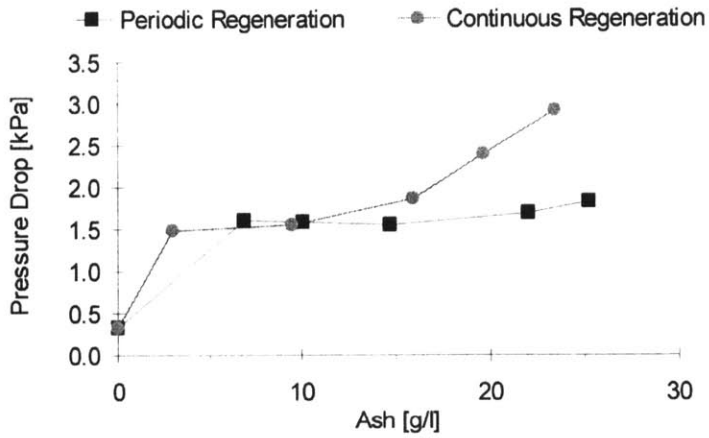

Figure 1-4 – Typical DPF Pressure Drop Response to Ash Load at 20,000hr^{-1} space velocity. DPF parameters: 6inL x 5.66inD, 200CPSI, 0.12in wall thickness. [21]

1.3.7.1 Wall Flow Monolith DPF

Several variations on the DPF have been researched and implemented. The primary on-road DPF configuration in use today is the wall flow monolith filter. The substrate of a wall flow monolith DPF is similar to that of a TWC. The DPF starts with an extruded honeycomb structure. It is converted from a flow through to a wall flow device by blocking one end of each flow channel in an alternating checker board pattern at the inlet and outlet faces. This creates inlet and outlet channels open to either the inlet or outlet flow, but not both. Exhaust gas is forced to flow through the porous walls of the honeycomb to pass from an inlet channel to an adjacent outlet channel. PM is filtered from the exhaust gas flow and trapped in the porous network of the channel walls or is deposited on the wall surfaces inside the inlet channels. The flow path and filtration mechanism is shown in Figure 1-5.

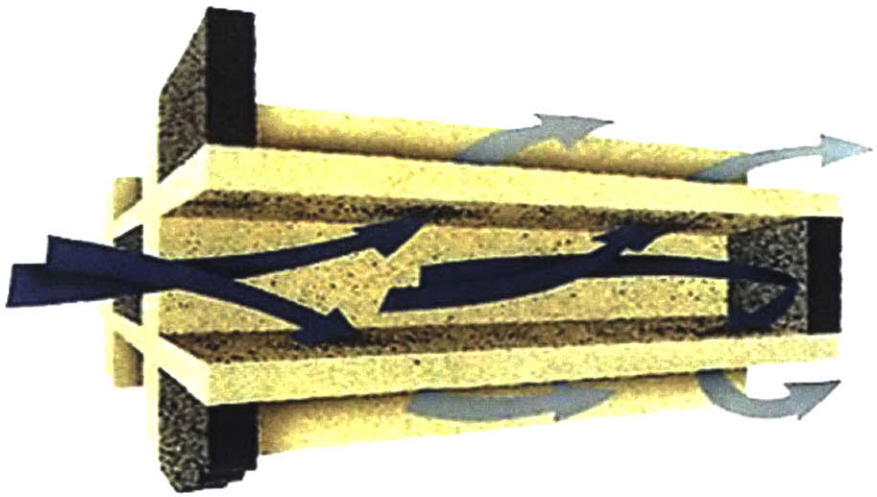

Figure 1-5 – Flow Pattern in a Wall Flow Monolith Filter. Pre-filtration gasses shown in dark blue, post-filtration shown in light blue. [22]

1.3.7.2 Regeneration of Wall Flow Monolith DPF

Soot that accumulates in a DPF is removed through oxidation in a process called regeneration. DPF regeneration strategies are characterized in two ways, periodic or continuous and oxygen or NO_2 driven. In all cases, regeneration requires sufficient levels of oxidizer and sufficient temperatures to initiate the chemical oxidation of soot in the DPF. Diesel engines operate fuel lean and generate significant NO_X emissions at all operating points. Excess oxygen is present in the exhaust stream for lean operation and NO_X can be converted to NO_2 by an oxidation catalyst

meaning that sufficient oxidizer is normally present in the DPF regardless of the oxidation driver used. Therefore DPF regeneration chemistry is temperature limited.

Periodic regeneration entails accumulation of soot in the DPF over a period with minimal soot oxidation. Eventually the accumulated soot is removed from the filter during a finite regeneration period. In this case regeneration is initiated by an increase in the filter temperature above the threshold temperature required for the soot oxidation reaction to commence. The threshold temperature is dependent on the chemistry of the soot oxidation, which will be discussed further with respect to oxygen versus NO_X driven regeneration. The increase in temperature to initiate a periodic regeneration can be the result of explicit engine operation routines designed to elevate exhaust temperatures to initiate regeneration or can be the result of normal fluctuations in exhaust temperature across a normal driving cycle [23].

Continuous regeneration requires that the DPF temperature is maintained above the threshold temperature for the applicable oxidation reaction at all times, and below the NO_X thermal equilibrium temperature for NO_X driven regeneration. Soot reacts with the oxidizer continuously as it is trapped in the DPF. No significant soot accumulation occurs in the DPF during continuous regeneration [23].

Oxygen driven regeneration relies on oxygen as the soot oxidizer. This regeneration type is analogous to the term active regeneration used in literature. The term "active regeneration" is not used here to remove ambiguity regard the root cause of the regeneration event. The minimum temperature required for rapid oxidation of soot with oxygen is $600^{O}C$ [23]. In diesel applications this normally requires a regeneration system or engine operation strategy that artificially increase the DPF inlet temperature (this is the origin of the term active). This regeneration strategy has grown less common in DPF applications due to development of NO_X driven regeneration methods because of the efficiency loss associated with adding energy to the exhaust stream to increase temperature.

NO_X driven regeneration relies on NO_2 as the soot oxidizer. This regeneration type is analogous to the term passive regeneration used in literature because active measures are not required to

elevate exhaust temperatures for regeneration. The minimum temperature required for rapid soot oxidation with NO_2 is $350^{O}C$ [23]. The lower temperature required for regeneration can more realistically be achieved for diesel engines without adding additional energy to the engine exhaust stream, however sufficient levels of NO_2 are not naturally occurring in the engine exhaust stream. An oxidation catalyst is required to convert NO to NO_2 to generate sufficient oxidizer levels for NO_X driven regeneration. A diesel oxidation catalyst (DOC) can be installed upstream of the DPF to generate NO_2 and/or oxidation catalyst can be applied directly to the DPF substrate to generate NO_2 in the filter. Soot oxidation in the DPF will return NO_2 to NO, which can then be removed from the exhaust stream by a NO_X trapping/reducing device located downstream of the DPF if needed.

1.3.7.3 Typical DPF Materials

Cordierite and Silicon Carbide are the two primary materials used in DPF substrates. Both materials have favorable thermal and porous properties. Silicon Carbide is more resistant to high temperatures with a sublimation temperature of $2400^{O}C$ compared with the $1450^{O}C$ melting temperature of Cordierite [22]. Cordierite offers better thermal shock resistance and lower cost. An additional drawback of Silicon Carbide is that its higher heat capacity and thermal conductivity may prevent self-sustaining regeneration at marginal exhaust temperatures because the exothermic energy of the soot oxidation cannot effectively raise the local temperature of the DPF [22].

1.3.8 Gasoline Particulate Filter Concept of Operation

Wall flow monolith filters are proposed as one possible option to reduce PM and PN emissions from GDI vehicles to meet Tier 3 and Euro 6 standards [24]. The filtration mechanism for a wall flow gasoline particulate filter (GPF) is identical to that of a DPF. The proven filtration efficiency of this mechanism in diesel applications is sufficient to achieve the PM emission reductions required for implementation of GDI engines [24]. However, it has been suggested that PM emissions can possibly be reduced to meet regulatory limits through engine design and operation strategies without a GPF [16, 8]. Additionally, gasoline engine performance and efficiency are more sensitive to increases in exhaust pressure than diesel engines. Therefore, it is important to fully understand GPF pressure drop performance and associated losses in engine

output and fuel efficiency across its entire service life before implementing GPF as a particulate emissions reduction strategy.

Pressure drop due to soot accumulation is normally more pronounced than pressure drop due to ash deposits per unit mass of material; however, soot accumulation levels can be controlled through regeneration strategies. Ash deposits cannot be easily removed from the GPF. The irreversible pressure drop increase caused by ash deposits must be understood to determine the expected full service life performance of the filter.

1.3.8.1 GPF Installation Location

Two installation locations are proposed for GPF. The underbody position locates the GPF beneath the vehicle chassis in-line with the exhaust piping upstream of the muffler. The close-coupled position places the GPF inside the engine compartment coupled directly downstream of the TWC. These positions each have advantages and disadvantages for ease of installation and maintenance access, but the primary characteristic impacting GPF performance is the significant difference in average and peak GPF inlet temperatures for the two positions. Peak inlet temperatures above $900^{O}C$ are possible in the close-coupled position. Peak inlet temperatures in the underbody position are expected to be below $700^{O}C$ contingent of exhaust system design. Average temperatures must be maintained at sufficient levels to achieve the regeneration threshold temperature for the oxidation reaction desired; otherwise additional energy must be expended to elevate exhaust temperatures invoking an overall fuel efficiency reduction. Peak filter temperatures resulting from the combination of peak inlet gas temperature and temperature rise from exothermic soot oxidation within the GPF must be maintained below the maximum operating temperature of the GPF substrate. Peak filter temperatures above $1000^{O}C$ can also cause detrimental changes in ash deposit morphology that will lead to significant increases in filter pressure drop [25].

1.3.8.2 GPF Regeneration Strategies

Regeneration of soot accumulated in a GPF follows the same chemical processes used in DPF regeneration. The first important distinction between GPF and DPF regeneration strategies is that gasoline engines operate at a stoichiometric AFR to facilitate proper operation of the TWC. The

excess oxygen present in diesel exhaust is not present in the gasoline case meaning that GPF regeneration strategies must provide sufficient temperature to initiate chemical reaction and elevated oxidizer levels in order for regeneration to proceed.

NO_X driven soot oxidation utilized in DPF applications relies on an oxidation catalyst upstream of or in the DPF to generate NO_2. The NO_2 generation in NO_X driven regeneration would conflicts with the NO_X reduction that occurs in the TWC, therefore oxygen is the preferred oxidizer for GPF regeneration.

The gasoline engine must operate at a stoichiometric AFR for all power producing operating points to meet gaseous emissions standards through proper operation of the TWC. This means that continuous GPF regeneration is not feasible due to a lack of oxygen. These factors point to periodic oxygen driven regeneration as the ideal regeneration strategy for GPF.

Periodic oxygen driven regeneration in the GPF requires temperatures greater than $600^{O}C$ and oxygen concentrations well above typical stoichiometric exhaust conditions to sustain soot oxidation [26]. GDI exhaust temperatures average 650-$800^{O}C$ [10]. Through proper exhaust system design, the GPF inlet temperatures can be maintained above $600^{O}C$ in the close-coupled or underbody positions when the engine operates under load. In marginal temperature conditions, energy added by the exothermic soot oxidation will sustain regeneration after it commences. The AFR must be modified to provide sufficient oxygen in the exhaust stream to initiate GPF regeneration. This can be achieved by stopping fuel injection during deceleration or coasting [24]. During these short periods of zero power demand fresh air is pumped through some or all of the engine cylinders and supplied to the exhaust stream. Provided that the GPF is at or above the regeneration threshold temperature, the resulting oxygen pulse will result in rapid oxidation of soot accumulated in the GPF. This regeneration strategy provides frequent periodic regenerations that will limit peak soot accumulation levels, limiting soot related GPF pressure drop.

1.3.8.3 Three-way Catalyst Coating of GPF

GPF researchers are currently experimenting with adding TWC coatings to GPF substrates [24, 27]. Full integration of TWC coating in a future GPF design has potential to reduce production cost and total exhaust system back pressure by removing the current TWC substrate and housing from the system. Wall flow monolith filters have been coated with catalysts for DPF applications providing foundational knowledge on the impact of coating on filtration, pressure drop, and structural strength in DPFs [28]. Catalyzed DPFs however have been designed to promote oxidation only. Further understanding of the impact of PM deposits on TWC coatings is needed to confirm that TWC coating in a GPF will be able to provide sufficient reduction of CO, HC, and NO_X to meet gaseous emissions limits throughout the GPF's service life.

(This Page Intentionally Left Blank)

2. Experimental Plan

The impact of incombustible ash deposits on GPF performance must be understood to provide for proper design and operation of GPF systems to minimize impact on engine output and efficiency. A full understanding of ash deposit formation mechanisms in GPFs and how ash deposits generate irreversible increases in pressure drop could give way to strategies to influence ash deposition to improve GPF performance throughout its service life. Ash deposits have also been shown to impact the effectiveness of catalyst coatings inside DPFs [28]. If TWC coatings are to applied to GPFs it is important to determine the possible reduction in catalyst effectiveness during the filter service life to ensure that all gaseous emissions limits can be met up to the regulatory end of service life of 150,000 road miles set forth in Tier 3 standards [5].

2.1 Accelerated Filter Loading

Close control of filter operating conditions and a short cycle time for aging GPF samples from new to end of service life is required to determine the effect of varied GPF configurations and exhaust conditions on ash deposition and GPF performance. A primary objective of this project is to generate laboratory-aged GPF samples using an accelerated ash loading system. The accelerated loading system facilitates loading GPF samples with oil-derived ash in a highly controlled environment. Filters are loaded in a shorter time span than filters aged on vehicles operating in the field or filters aged with normal exhaust from laboratory engine running on a dynamometer.

2.1.1 Experimental Apparatus

Several accelerated loading techniques are utilized to generate laboratory aged filter samples in DPF and GPF research [29, 30]. Fuel can be doped with oil to ensure in cylinder combustion of the test oil and entrainment of oil derived ash in the engine exhaust [29]. Test oil can also be injected into the air intake manifold to accelerate ash deposition in the test filter [30]. To improve on these methods a novel system for accelerated ash loading of DPFs was developed in [31]. This system utilizes a burner system that generates exhaust gasses. Lubricating oil is injected into the burner combustion chamber to create elevated levels of lubricant derived ash in the exhaust stream flowing to the test filter. A new accelerated aging system is used for this GPF

research. It is based on the system outlined in [31] and modified for GPF research. Development of the system is outlined in [32].

The accelerated aging system is shown in Figure 2-1. The system consists of a furnace burner (4) modified to burn gasoline provided by a 30 gallon fuel cell (3). The flame is sustained by three spark plugs (5) that provide continuous ignition. The burner flame is directed into the combustion chamber (6). An air assisted oil injection nozzle (15) located on the cover of the combustion chamber injects oil into the chamber. The oil is burned in the chamber releasing lubricant derived ash into the exhaust stream.

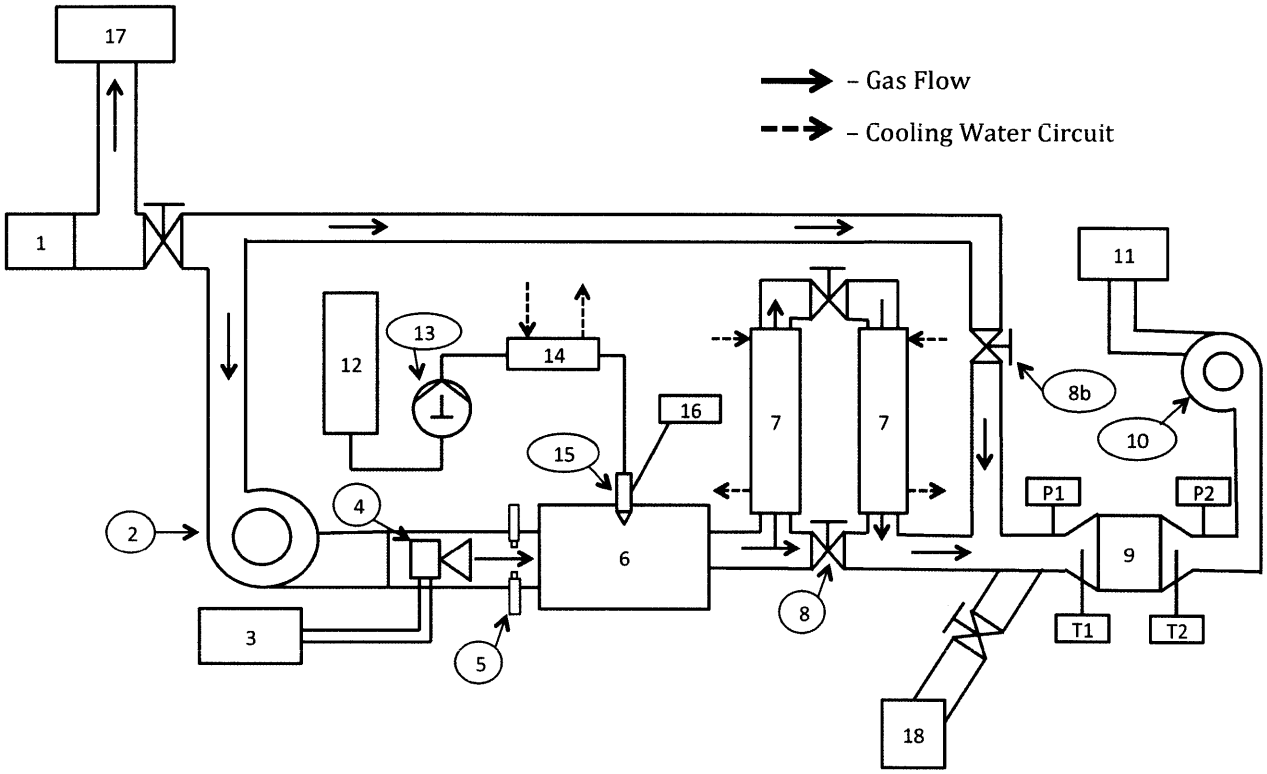

Figure 2-1 – GPF Accelerated Ash Loading System with Parallel Dyno Test Engine

1 – Inline Airflow Sensor
2 – Burner System Integral Fan
3 – Fuel Cell
4 – Burner System
5 – Continuous Spark Igniters
6 – Combustion Chamber
7 – Exhaust Gas Cooler
8 – Temperature Control By-pass Valve
8b – Secondary Air Inlet Valve
9 – Test GPF
10 – Centrifugal Blower
11 – Exhaust Trench
12 – Test Oil Reservoir
13 – Fluid Metering Oil Pump
14 – Oil Cooler
15 – Air Assisted Oil Injection Nozzle
16 – Compressed Air Supply
17 – Air Supply to Test Engine
18 – Exhaust Inlet from Test Engine

The temperature of the exhaust stream is controlled by adjusting a by-pass valve (8) that directs hot gas through a water-cooled heat exchanger (7) when closed. The balance between exhaust gases passing through and by-passing the cooler determines the temperature at the filter inlet. A secondary air inlet valve (8b) located between the exhaust stream cooler and the test filter (9) can be opened to increase the oxygen level in the exhaust stream.

The exhaust stream temperature is monitored along the exhaust flow path to determine proper operation of the system. The GPF inlet (T1) and exhaust (T2) temperatures are measured in the inlet and outlet cones of the filter canister to characterize the filter temperature and inlet flow conditions. The static pressure is measured upstream (P1) and downstream (P2) of the GPF to measure the pressure drop across the filter. Pressure drop across the filter is monitored during all system operations, but all official pressure drop data is taken at room temperature with the burner offline to maintain a consistent reference air density. Flow through the system is generated by a centrifugal blower (10) at the system outlet. During burner operation, an integral fan in the burner system (2) generates additional flow.

The accelerated aging system includes several modifications from the original form discussed in [32]. The system is capable of delivering stoichiometric exhaust to the filter inlet in an attempt to replicate the chemical environment in which ash agglomerates form from the ash precursors contained in the exhaust stream. For a given fuel injection configuration there is a small envelope of airflow rates that can be achieved while maintaining stoichiometric exhaust conditions. The oxygen level in the exhaust stream can be elevated by raising the centrifugal blower speed to raise the airflow rate through the burner. Short duration oxygen rich exhaust pulses simulate the deceleration and coasting regeneration strategy discussed in section 1.3.8.2.

The accelerated aging system is installed alongside a 1.6L Ford EcoBoost engine typical of the 2013 Ford Escape. The EcoBoost is a GTDI engine capable of producing peak power of 178hp at 5700rpm and peak torque of 184lb-ft at 2500rpm. Exhaust gases from the engine can be directed to the filter installed on the accelerated aging system for soot loading and engine performance testing.

The exhaust ducting connecting the engine to the filter housing on the accelerated aging system is longer than the typical exhaust system in the current laboratory configuration. The excess ducting results in lower filter inlet temperatures than expected for the underbody position. There is no mechanism to control filter inlet temperature independent of the engine exhaust temperature when operating the test engine. Increasing the filter inlet temperature relative to engine exhaust temperatures and introducing temperature control independent of exhaust manifold temperature are possible future improvements for this experimental apparatus.

2.1.2 Loading Procedures

Two groups of GPFs were aged on the accelerated aging system. Un-catalyzed cordierite filter substrates were used for loading Experiments 1 and 2. Cordierite filters with a three-way catalyst coating were used for loading Experiment 3. The filter characteristics are given in Table 2-1.

Table 2-1 – Test GPF Characteristics

Un-catalyzed Filter Parameters	
Length (in)	5.51
Diameter (in)	4.66
Channel Density (CPSI)	220
Volume (L)	1.54
Catalyst Coating	None
Porosity	48%
Mean Pore Size	12μm

Experiment 3 GPF Parameters	
Length (in)	5.0
Diameter (in)	5.19
Channel Density (CPSI)	300
Volume (L)	1.73
Catalyst Coating	TWC
Porosity	30%
Mean Pore Size	15.7μm

For loading Experiments 1 and 3, a series of filters were loaded under the same conditions to various terminal ash loads. GPF samples with a range of terminal ash loads were created so that destructive testing can be completed on samples representing various stages of the GPF service life. The fundamental measure of filter age in this study is grams of ash present in the filter per liter of filter volume. Equation 7 is used to calculate terminal ash load for a filter based on the target simulated road mileage.

$$AL = \frac{OilCons * \rho_{oil} * \tilde{x}_{ash}}{V_{filter}} * FR_{ash} * Mi_{sim} \quad (7)$$

AL - Target Ash Load (g/L)
OilCons - Engine Oil Consumption (quart/mile)
ρ_{oil} - Oil Density (g/m3)
$\tilde{x}_{ash}$ - Mass Fraction Incombustible Ash in Test Oil
V_{filter} - Filter Volume (L)
FR_{ash} - Ash Finding Rate
Mi_{sim} - Simulated Road Mile

The first term of equation 7 determines the theoretical rate of oil-derived ash in the exhaust stream based on engine and oil characteristics and normalized to the filter volume. Research has shown that this theoretical rate of ash emission from the engine overestimates the rate at which ash is found to deposit in particulate filters in experimental tests. The ratio of actual ash loading rate to theoretical ash emission rate is known as the ash finding rate. Finding rates ranging from 3-67% have been reported in literature [33, 34]. The assumed finding rate for this experiment was calculated based on the concentration of individual oil additives in the test oil, determined through ASTM D874, and finding rates for individual additives reported in [33]. Table 2-2 summarizes the assumed values of equation 7 variables and their source.

Table 2-2 – Target Ash Load Calculation; Assumed Values

Ash Load Calculation; Assumed Values		
Input	**Value**	**Source**
Oil Consupmtion	**0.0001 (quart/mil)**	**Engine OEM**
Oil Density	**877 (kg/m^3)**	**Measured**
Oil Mass Fraction Ash	**0.0102**	**ASTM D874**
Un-catalyzed Filter Volume	**1.54 (L)**	**Measured**
Catalyzed Filter Volume	**1.73 (L)**	**Measured**
Ash Finding Rate	**37%**	**[33]**

The target ash loads for Experiments 1, 2, and 3 were calculated using equation 1 and are given in Table 2-3. Each sample GPF was assigned a filter designation consisting of a number only for un-catalyzed filters and a number preceded by the letter "C" for catalyzed filters.

The four catalyzed GPF (C-GPF) loaded in Experiment 3 had catalyst particle densities of either $3g/ft^3$ or $10g/ft^3$. The catalyst load for each filter in Experiment 3 is listed in Table 2-3. The cordierite substrates and wash coat were identical across all C-GPFs meaning that the variation in catalyst load did not impact the flow resistance of the filters.

Electron microscope imaging of the C-GPF substrate does show two fundamental differences between these C-GPFs and catalyzed DPFs analyzed in the past. The wash coat volume is higher in the C-GPFs and the penetration through the porous network of the channel wall is higher. Catalyzed DPFs often have thin layers of wash coat that is only present at the inlet and outlet channel surfaces and penetrates into the porous network by 10% of the wall thickness. The wash

coat in a catalyzed DPF causes small decreases in the overall filter porosity. In the C-GPFs tested, large volumes of wash coat are present through the entire thickness of the filter walls. The porosity of the filter decreases by 50% due to the presence of wash coat compared to the bare cordierite porosity before coating. Full penetration of the wash coat also means that catalyst particles are distributed throughout the wall thickness, not just at the inlet and outlet surfaces of the wall.

Table 2-3 - Target Ash Loads for Experiments 1, 2, and 3

Experiment	Filter	Final Ash Load (g/L)	Equivalent Miles
1	1	3	15,000
1	2	6.1	30,000
1	3	12.2	60,000
1	4	20.3	100,000
1 & 2	5	30.5	150,000

Experiment	Filter	Final Ash Load (g/L)	Equivalent Miles	Catalyst Load
3	CC	0	0	10 g/ft^3
3	C1	3.6	20,000	3 g/ft^3
3	C2	6.3	35,000	10 g/ft^3
3	C3	12.6	70,000	3 g/ft^3
3	C4	20	110,000	10 g/ft^3

Filter CC is a clean catalyzed filter sample that was not loaded with ash in the accelerated aging system. It was used as a clean filter baseline for catalytic activity testing discussed in section 2.2. The catalyst load for filter CC is 10g/ft^3

In Experiment 2 filter 5 was loaded with soot at predetermined ash levels to track the impact of ash load on the GPF's pressure drop response to soot. At each 5g/L of ash load, a soot loading cycle was completed. The filter was loaded to 3g/L of soot at 0.5g/L increments. Pressure drop measurements were conducted for each soot loading increment. The filter was regenerated at 600-650 degC after each soot loading cycle to remove all possible soot from the filter. Oil was not injected for ash deposition during these regeneration cycles. Any mass gain from the beginning of a soot loading cycle to the mass after regeneration was treated as new ash in the filter. Ash accumulation during soot loading cycles is attributed to ash from several hours of engine operation during a soot loading cycle and ash precursors previously deposited on the

loading system tubing walls and re-entrained into the exhaust stream during the soot loading and regeneration operations. The new ash accumulation averaged 0.3g/L ash per soot loading cycle.

Similar ash loading cycles were utilized for all loading experiments. Filters were loaded below soot oxidation temperatures for 3.5 hours at 375-425degC and regenerated at 600-650degC for 30 minutes. Oil was injected throughout the loading and regeneration cycle with a target ash-loading rate of 0.25g/L-hr for all experiments. The loading cycle parameters used for each loading experiment are outlined in Table 2-4.

Table 2-4 – Ash Loading Cycle

Test Cycle Parameters	
Primary Loading Period	**3 hr 30 min**
Loading Temp (degC)	**400**
Regeneration Period	**30 min**
Regeneration Temp (degC)	**600-650**
Flow Rate (SCFM)	**32-35**
Space Velocity (1/hr)	**35-38K**
Ash Loading Rate (g/L-hr)	**0.25**

The pressure drop across the filter is measured after each ash loading cycle or series of two loading cycles. The number of cycles between pressure drop measurements determines the resolution of pressure drop data with respect to ash load. Pressure drop measurements are always taken with the filter and airflow at room temperature, which ranged from 20-35^{O}C. Flow through the filter is driven entirely by the downstream centrifugal blower. The burner system and water-cooled heat exchanger are bypassed and isolated for all pressure drop measurements. The flow rate through the filter is varied from 0-80SCFM in 5-10SCFM steps by varying the blower speed. Airflow rate is measured at the system inlet and static pressures are measured immediately upstream and downstream of the GPF housing. Pressure drop across the filter is calculated and the resulting data is fit with a quadratic function to model pressure drop versus flow rate for the given filter ash loading level. Figure 2-2 shows raw data and quadratic fit lines for each pressure drop measurement for filter 1.

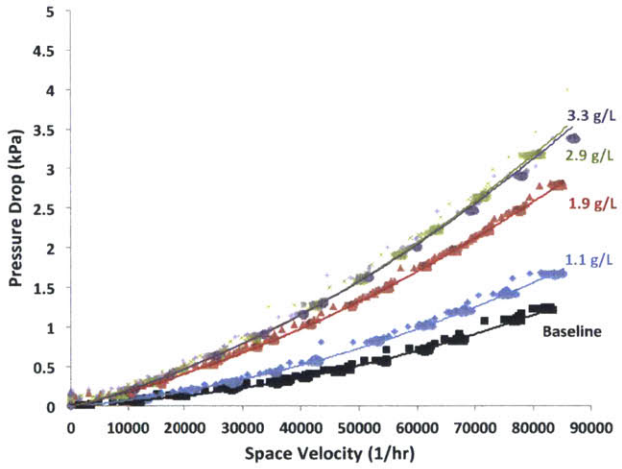

Figure 2-2 – Filter 1; Pressure Drop vs. Flow Rate for All Ash Loads

After loading, destructive testing was conducted for each GPF to characterize the nature of ash deposits at various points in a typical filter's service life. Repetition of identical loading conditions also allowed for direct comparison of the pressure drop trends for the various test filters to determine the impact of certain characteristics measured during destructive analysis and the level of variation in the random processes governing ash deposition for a given filter configuration.

2.2 Catalytic Activity Testing

TWC coating has been applied to experimental GPFs in an attempt to save cost and reduce the overall exhaust system backpressure [27]. Studies have demonstrated a reduction in catalyst efficiency for flow through TWCs [35] and catalyzed DPFs [28] due to deposits of ash and other materials from exhaust gases. The impact of ash deposits on the catalytic effectiveness for filters aged in loading Experiment 3 was tested to characterize the reduction in C-GPF performance attributable to ash loading.

2.2.1 Catalyst Test Bench

A gas reactor flow bench was used to test the catalytic activity of C-GPF samples aged on the accelerated aging system. The test bench arrangement is shown in Figure 2-3. The bench consists of a feed gas manifold, inline flow heater, and two heated insulators. Calibrated inlet gasses are delivered to a test section at the desired flow rate and temperature. A MKS Instruments Multigas

Model 2030HS Fourier Transform Infrared Spectroscopy gas analyzer (FTIR) samples upstream of the test section to calibrate the inlet gas composition and downstream of the test section to determine the products of reactions occurring in the test section.

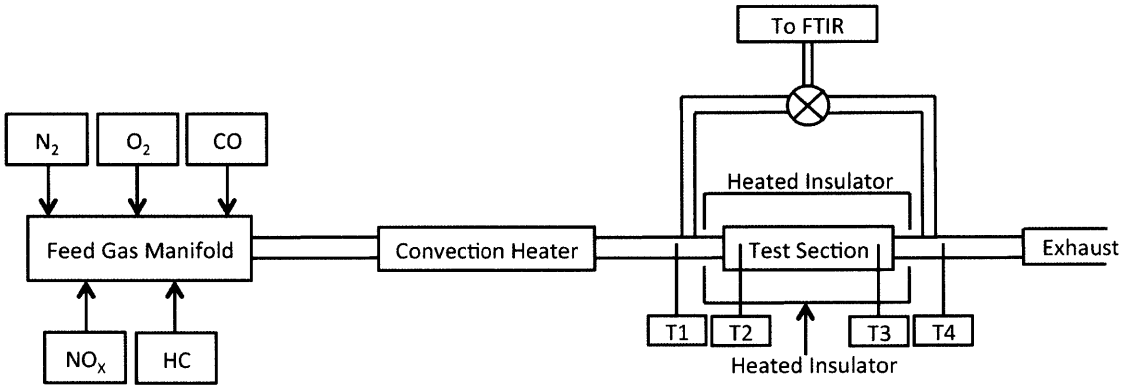

Figure 2-3 – Catalyst Reactor Test Bench Arrangement

2.2.2. Test Procedure

Core samples of each aged C-GPF were canned in removable test sections. Insulating matting sealed the sample in the test section to force all flow through the filter walls. The light-off temperature of the three-way catalytic reactions was determined using a temperature ramp experiment for two exhaust conditions. The lean light-off temperature of the oxidation reactions was measured using an oxygen rich inlet gas composition. The near-stoichiometric light-off temperature of the oxidation and reduction reactions was measured using a low oxygen inlet gas composition. Table 2-5 lists the inlet gas composition for lean light-off and near stoichiometric experiments.

Table 2-5 – Inlet Gas Composition for Catalyst Light-off Experiments

Lean Light-off	
Gas	**Inlet Concentration**
CO	**500 ppm**
HC	**500 ppm**
NO	**500 ppm**
O2	**5%**
N2	**Balance**

Near-Stoichiometric Light-off	
Gas	**Inlet Concentration**
CO	**1000 ppm**
HC	**500 ppm**
NO	**500 ppm**
O2	**1000 ppm**
N2	**Balance**

To determine the light-off temperature, the filter samples were exposed to a steady stream of inlet gases at a space velocity 45,000hr^{-1} while the inline flow heater and heated insulators

ramped the flow temperature from room temperature to 600degC. The FTIR sampled the outlet gas composition downstream of the test section during the temperature ramp and recorded the levels of CO, CO_2, O_2, NO, NO_2, H_2O, and Propylene in the outlet gas stream. The temperature ramp rate was 10 degrees per minute. The filter temperature was characterized as the average of the gas temperatures at the test section inlet and outlet measured by thermocouples centered in the gas stream.

Figures 2-4 and 2-5 show examples of the outlet gas composition plotted versus filter temperature for lean and near-stoichiometric light-off temperature ramp experiments. For each experiment, the light-off temperature of each catalyzed reaction was characterized as the temperature at which there was a 10% reduction in the relevant reactant. Full results are discussed in section 4.2.

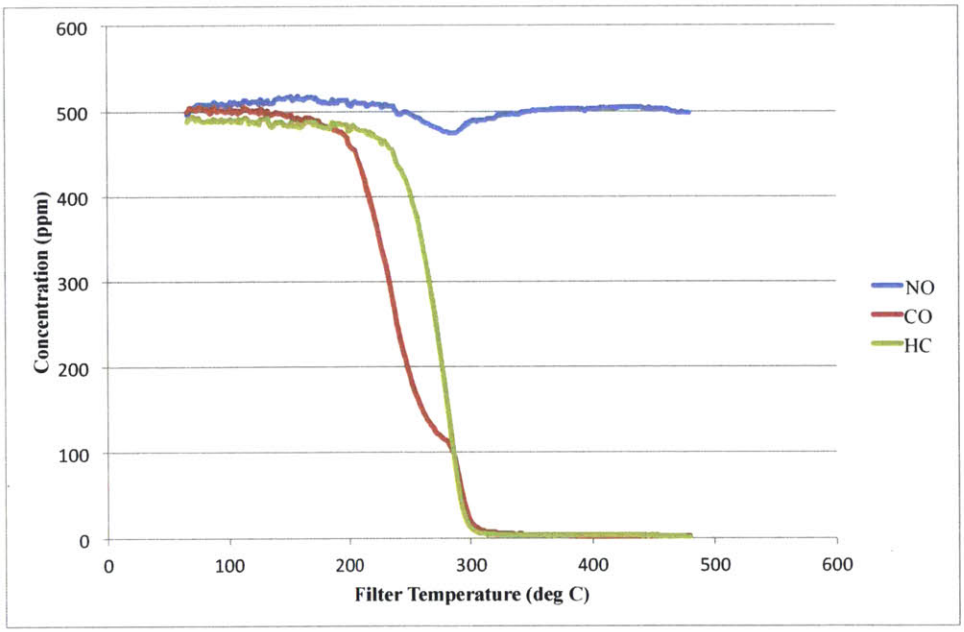

Figure 2-4 – Example Temperature Ramp Experiment Results; Zero Ash, Lean Exhaust

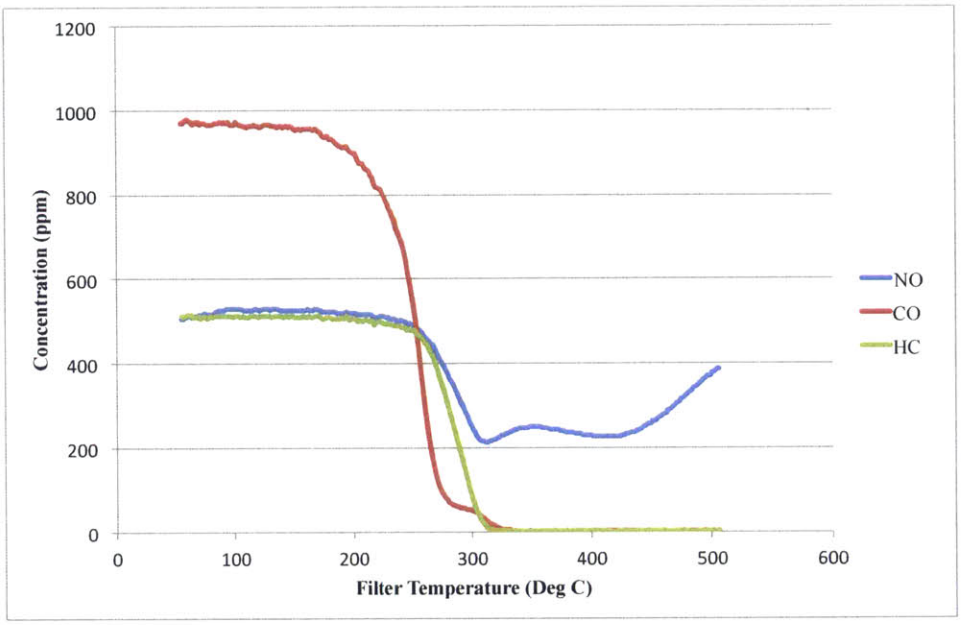

Figure 2-5 – Example Temperature Ramp Experiment Results; Zero Ash, Near-stoichiometric Exhaust

(This Page Intentionally Left Blank)

3. Ash Distribution

There are two primary locations where ash deposits form in a wall flow monolith filter. Ash layers form on the inlet channel walls and grow in thickness during the life of the filter as ash precursors are filtered from the exhaust gasses flowing through the filter walls. Some ash deposits will break free of the wall layer and move towards the outlet end of the filter forming an ash plug at the rear of the inlet channels. Soot deposits that form in the filter between regenerations will predominantly form a wall layer but under certain conditions a distinguishable soot plug is possible [36]. Figure 3-1 demonstrates these two ash accumulation locations and the similar soot accumulations that form on top of the underlying ash deposits between regeneration events.

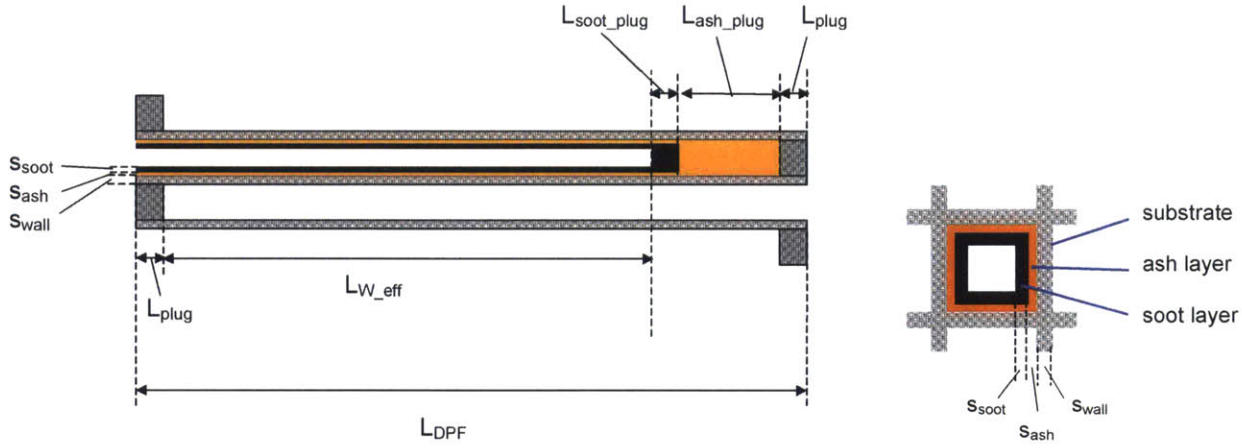

Figure 3-1 - Ash and Soot Deposit Types and Locations within an Inlet Channel [36]

3.1 Impact of Wall Layer versus Ash Plug Deposits

Research in ash impacts on DPF performance have shown that ash mass located in the ash plug section will have a smaller impact of DPF pressure drop than ash mass deposited in wall layers [34]. The primary mechanism for increased pressure drop due to the ash plug is a reduction in filtration area. As the ash plug grows, the wall area covered by the solid deposit is effectively removed from the filter's overall filtration area. Depending on the cross sectional area of the inlet channels and the packing density of the ash plug area, a significant mass of ash can be stored in an ash plug per unit length of lost inlet channel walls.

Ash deposited in the wall layer forms a new porous structure on the surface of the porous filter wall and acts as an additional filter element. Exhaust gasses must flow through this additional porous layer increasing the overall flow resistance for flow through the filter walls. The wall layer thickness increases as ash is added, increasing the flow resistance of the layer.

At very high ash loads the geometric impact of growing ash plugs and very thick wall layers begins to accelerate the rise in pressure drop relative to ash load. Effective filtration area is reduced by growth of the ash plug throughout the filter's service life. At high loads the wall layer deposits also begin to reduce effective filtration area because the inlet channel corners are filled in by ash and the cross section of the open area transitions from square to circular. This type of ash deposit is shown in Figure 3-2, which shows a DPF loaded to 42g/L of ash. These effects impact heavy duty diesel DPFs towards the end of their 200,000 to 250,000 road mile service life, but may have a reduced impact on GPFs with shorter expected services lives of 150,00 to 200,000 miles.

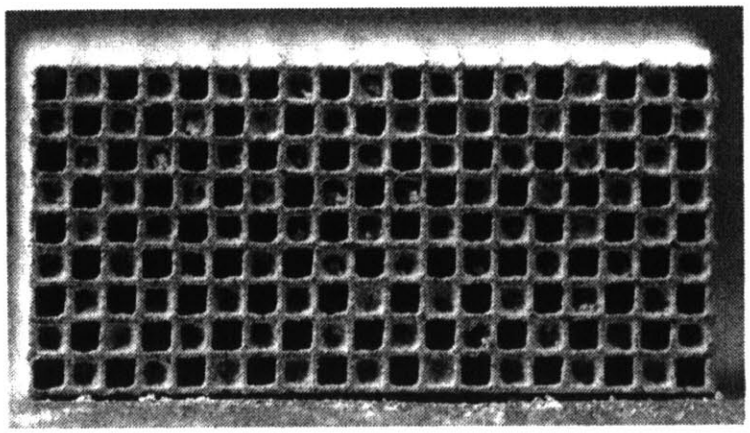

Figure 3-2 – DPF Loaded to 42g/L Ash in DPF Accelerated Aging System [21]

3.2 Characterization of Ash Distribution in Test Samples

The wall layer thickness and ash plug volume present in aged GPF samples were characterized through manual measurements. Core samples of approximately 80 channels (40 each inlet and outlet) were cut from un-catalyzed filter samples 4 and 5. These core samples were sectioned longitudinally into four sub-sections. The front and rear faces of each section were photographed

for image analysis to determine the ash layer thickness at the longitudinal position of the cut. Figure 3-3 shows examples of a core sample and sample sub-sections.

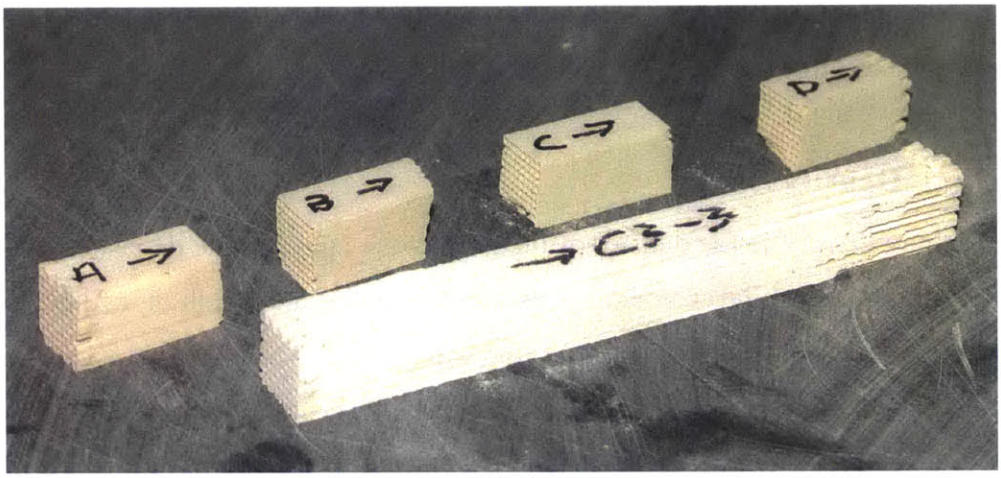

Figure 3-3 - GPF Core Sample C3-3 and Sub-section A through D for Analysis

The photographs of the front and rear face of each sample sub-section were analyzed using Image-J software to measure the horizontal and vertical dimension of the open area remaining in each inlet channel. The remaining open dimension was subtracted from the initial channel open area to determine the ash layer thickness for the channel in question. The calculated wall layer thicknesses for each inlet channel were averaged to determine the mean wall layer thickness for that sample at the longitudinal location of the cut. Figure 3-4 shows an example of a sub-section face photograph and the measurements taken in Image-J.

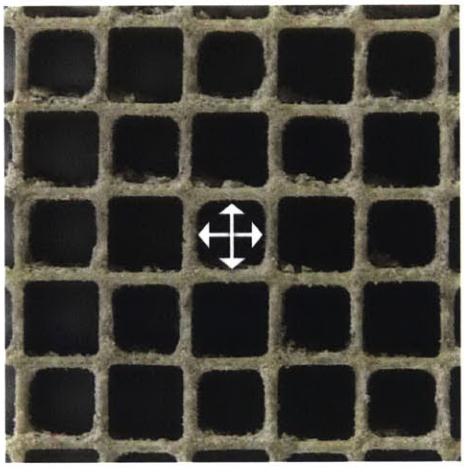

Figure 3-4 - Example of GPF Sub-section Photo for Image-J Analysis. White Arrows Show Dimensions Measured in Image-J.

The ash plug length was determined using a depth gauge to measure from the front face of the rear sample sub-section to the forward end of the ash plug. Ash plug depths for each inlet channel were averaged to find the mean plug depth. The sub-section overall length and the length of the ceramic inlet channel end block were used to convert from measured ash plug depth to plug length to determine the ash plug volume.

3.3 Packing Density

The ash packing density is the density of the porous ash agglomerate deposited within the GPF. After determining the ash layer thickness distribution along the length of a filter sample and the ash plug length, the ash deposit volumes in the wall layer and ash plug were calculated. The ash deposit mass was estimated by comparing the mass of the filter sub-sections before and after removing the ash deposits of known volume. Ash deposits were removed from the sample sub-sections by five minutes of tapping to loosen ash deposits followed by purging with compressed air to remove as much ash as a possible. The packing density of the ash deposits was determined by dividing the estimated mass by the calculated ash volume.

Packing density is an important ash characteristic that relates to ash deposit permeability and filter pressure drop. By comparing the packing density of ash deposits in GPF samples loaded under different conditions it is possible to identify how different exhaust conditions, engine operation, and lubricant oil chemistries impact GPF performance. Packing density is also used to estimate the porosity of ash deposits for use in filtration models. The porosity of an ash agglomerate is found using equation 8 where P is the porosity, ρ_t is the theoretical density of the compounds present in the agglomerate, and ρ_p is the packing density.

$$P = 1 - \frac{\rho_t}{\rho_p} \tag{8}$$

4. Results

4.1 GPF Pressure Drop Performance

Using the quadratic pressure drop models generated from raw pressure drop data, a GPF's expected pressure drop at a given ash load can be calculated for any flow rate between 0 and 80SCFM. For a given flow rate or equivalent space velocity the pressure drop is plotted against ash load to represent the increase in pressure drop across the service life of the filter.

4.1.1 Un-catalyzed GPF

Figure 4-1 is a compilation plot of pressure drop versus ash load for Experiment 1. All filters are fully regenerated to remove soot prior to these measurements.

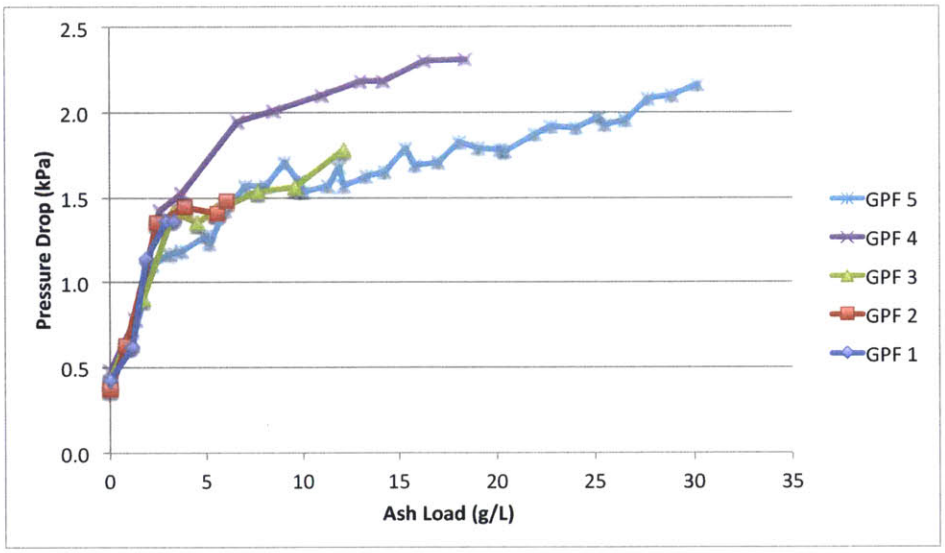

Figure 4-1 – Filter 1-5; Pressure Drop vs. Ash Load at Space Velocity 45,000 hr^{-1}

All filters follow the same steep slope during the first 3g/L of ash loading. This steep rise in filter pressure drop is associated with the deep bed filtration regime during which ash particles penetrate into the filter wall porous substrate reducing the wall's porosity and porous network connectivity. For ash loads greater than 8g/L filters 4 and 5 display similar slopes, 0.032 and 0.025 respectively. This area of reduced slope and linear pressure drop increase represents the cake layer filtration regime. In this regime ash builds up in a layer on the surface of the filter

walls causing an increase in pressure drop proportional to the thickness in the ash deposit layer. The ash plug also grows during this filtration regime increasing pressure drop due to reduction in effective filtration area.

The transition period between the deep bed and cake layer filtration regimes constitutes a third unique regime in the GPF pressure drop response to ash loading. During the transition period ash deposits begin to form on the inlet wall surface as other ash agglomerates continue to enter the filter wall pore structure. The initial ash deposits on the wall surface may not interfere directly with the exhaust gas flow path into the porous network of the filter wall.

Ash islands have been observed on the wall surface of moderately loaded GPF samples using Environmental Scanning Electron Microscope (ESEM) imaging. Figure 4-2 shows two examples of these initial ash layer deposits in filters 1 and 2, loaded to 3g/L and 6g/L ash load respectively.

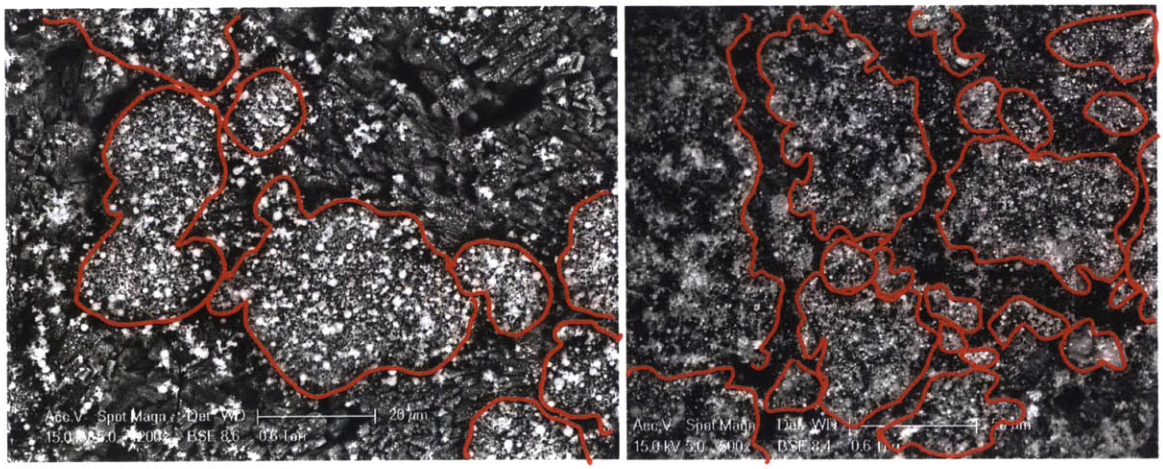

Figure 4-2 – Scanning Electron Microscope images of ash islands growing on the surface of inlet channel walls. LEFT; Filter 1 (3g/L Ash) shows evidence of ash island formation. RIGHT; Filter 2 (6g/L Ash) contains larger ash islands that are beginning to connect to form a uniform wall ash layer. Images courtesy of Dr. C.J. Kamp.

As the transition period proceeds, these ash islands will grow to cover the entire inlet channel surface, forming the ash wall layer, which will persist and grow for the remainder of the GPF's service life. The transition period effectively locks the pressure drop caused by deep bed filtration. The wall layer, once fully formed, will prevent significant transport of ash into or out of the filter wall porous network leaving changes in the volume and permeability of the wall

layer and ash plug as the only variables capable of influencing pressure drop for the remainder of the filter's service life. For Experiment 1, the transition zone occurs from 3g/L to 6g/L of ash load.

During the transition period between deep bed and cake layer filtration the pressure drop of filter 4 increases by 0.5kPa over the trajectory of the other 4 filters of Experiment 1. This 0.5kPa offset between filters 4 and 5 perpetuate for the remainder of the filters' life. This increase occurs between 20,000 and 40,000 road miles will reduce the system performance and efficiency for the remainder of the vehicles' service life.

The transition zone can be re-characterized by normalizing the ash volume to the total void space present in the subsurface layer of the porous filter walls. The penetration depth of ash deposits into the channel wall porous network defines the subsurface layer. For Experiments 1 and 3 the subsurface layer was found to be 30% of total wall thickness using scanning electron microscope imaging. The ash volume is determined based on the estimated apparent density of the ash agglomerates in the filter wall. Apparent density is assumed to be $0.3g/cm^3$.

After normalizing, the new x-axis ordinate is the theoretical percentage of the subsurface layer void space filled by the ash volume present. In reality ash deposits begin to form on the surface of the filter walls, outside of the wall's porous void volume, during the transition period and thereafter. However, normalizing to subsurface layer void volume isolates filter porosity and facilitates analysis of the impact of other filter and exhaust characteristics on the onset of the filtration mode transition zone. Figure 4-3 shows the pressure drop data from Experiment 1 normalized in this fashion. The transition zone occurs from 25% to 50% subsurface void volume filling.

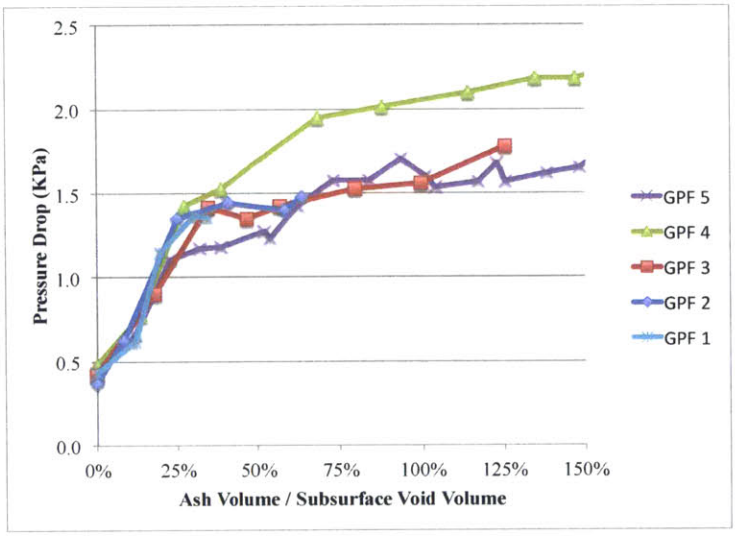

Figure 4-3 – Filters 1-5; Pressure Drop vs. % Subsurface Void Volume Filling at Space Velocity 45,000 hr^{-1}

4.1.2 Un-catalyzed GPF with Soot Loading

GPF 5 was loaded with up to 3g/L of soot seven times during its ash loading cycle. Figure 4-4 is a representation of the combined pressure drop impact of ash and soot across the full life of the GPF. The x-axis represents the sum of ash load and soot load for each pressure drop data point.

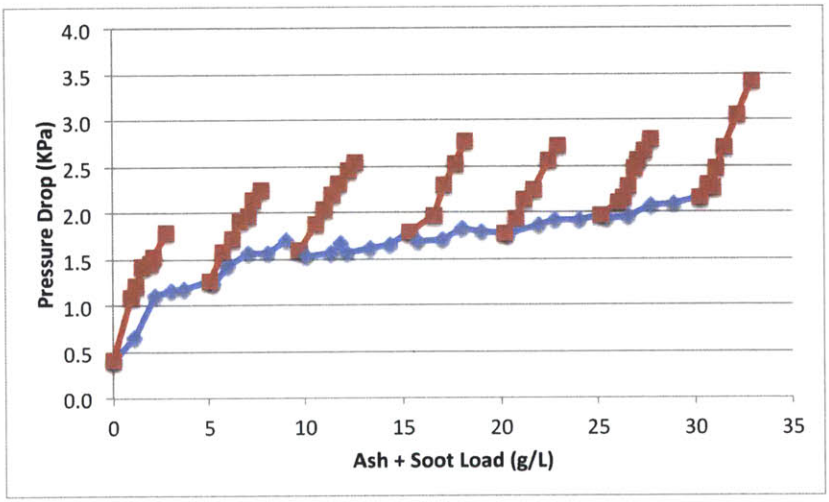

Figure 4-4 - Filter 5; Pressure Drop vs. Combined Ash + Soot Load at Space Velocity of 45,000 hr^{-1}

Previous DPF research has shown a bimodal response to soot loading for a clean filter with both deep bed and cake layer filtration regimes evident in the pressure drop response. As ash load increases the response to soot loading becomes more linear because the ash layer prevents deep

bed filtration of soot and cake filtration becomes the sole soot filtration mode. [37]. Elimination of soot depth filtration by the ash wall layer has been shown to have a net positive impact on DPF performance with an ash loaded filter creating a lower backpressure than a clean filter at equal soot loading levels [21].

In Figure 4-5 the pressure drop response for each soot loading cycle was re-plotted with absolute pressure drop versus soot load to identify any benefit resulting from ash wall layer formation.

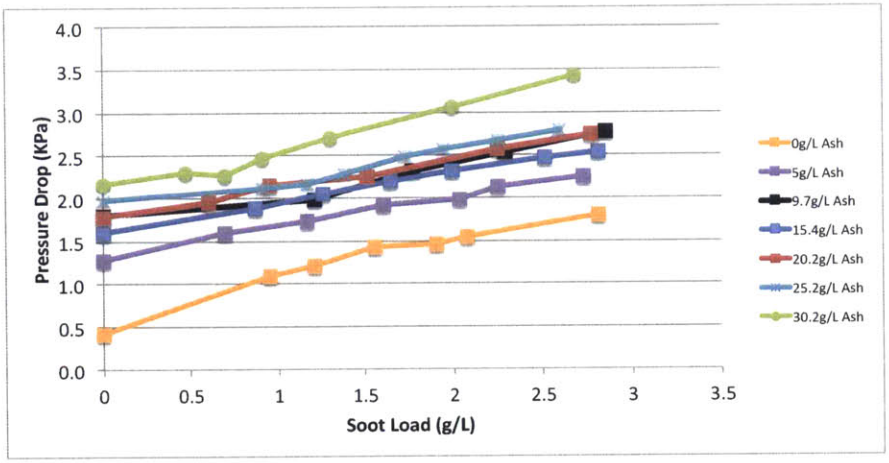

Figure 4-5 - Pressure Drop vs. Soot Load at 0-30g/L Ash Load at Space Velocity 45,000 hr^{-1}

A net benefit from early ash wall layer formation would be indicated if the 0g/L ash pressure drop curve crosses above the pressure drop curve for higher ash loads, but that result is not observed in this case. For pressure drop in the clean GPF to surpass the soot response for higher ash loads there must be a prolonged deep bed filtration of soot with a steep pressure drop response. Figures 4-5 and 4-6 demonstrate that a prolonged steep pressure drop response is not present in this case.

In Figure 4-6 the pressure drop response for each soot loading cycle is normalized by subtracting the soot free pressure drop at the given ash loading level. This isolates the pressure drop response to soot loading in order to identify changes to this response over the life of the filter.

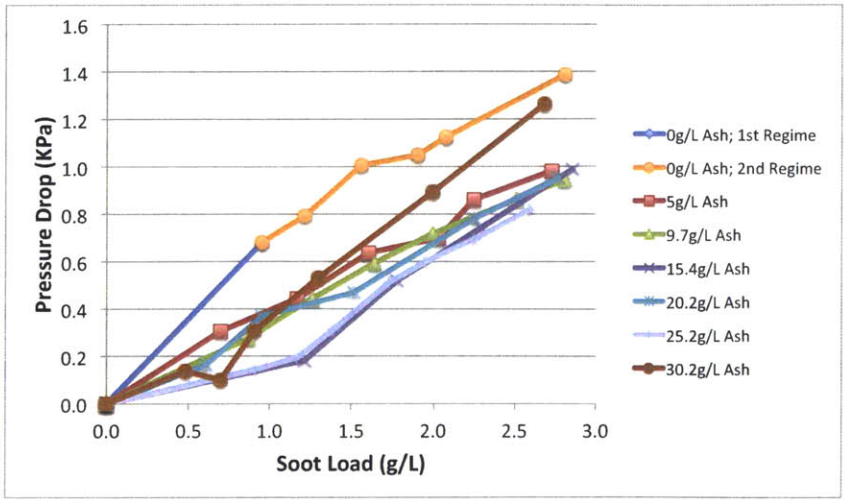

Figure 4-6 – Pressure Drop due to Soot Loading Only at 0-30g/L Ash at Space Velocity 45,000 hr^{-1}

Although a net benefit due to ash loading is not demonstrated in Figure 4-5, Figure 4-6 does show that ash loading prevents deep bed filtration of soot and reduces the pressure drop response to soot loading. Linear regression analysis of the response to soot loading at each ash level shows a consistent linear response for soot cake filtration with a response slope between 0.34 and 0.37 kPa per g/L. The responses for all ash loads from 5g/L to 25g/L show a single response mode with a slope in this range. The soot loading response for 0g/L ash shows a bimodal response with the second mode falling in the cake filtration regime with a slope of 0.37 above 0.9g/L soot. The first regime for the response at 0g/L ash has a slope of 0.7 between two data points. Unfortunately, the lack of pressure drop data points for soot loads below 0.9g/L soot in this data set make it impossible to identify either the true first regime response slope or the soot load level at which the regime transition occurs.

To satisfy a linear model of pressure drop response for soot cake filtration the y-intercept of the linear regression must be zero. R statistics software was used to determine the p-value of the y-intercept for linear regression of the soot response data for ash loads 5g/L to 25g/L. P-values are given in Table 4-1.

Table 4-1 – P-values for Hypothesis(Y-intercept = 0) for Soot Response as Ash Loads 5-30g/L

Ash Load (g/L)	Y-Int P-Value
5	0.9
10	0.816
15	0.408
20	0.706
25	0.118
30	0.0832

The hypothesis that the soot response y-intercept is equal to zero cannot be rejected at a 90% confidence level for ash loads 5g/L to 25g/L. This supports the single mode linear response model proposed. At 30g/L the hypothesis is rejected at a 90% confidence level. This is consistent with the previous observation that the proposed soot response model does not apply at this ash load due to the onset of geometric effects due to high ash load.

The final soot loading cycle conducted at 30g/L ash shows a steeper response. This can be associated with geometric effects that cause reductions in filtration area within the filter at higher ash loads as discussed in section 3.1 [21]. It is important to note that these effects only appear after 150,000 simulated road miles as the GPF is approaching the end of its expected service life.

4.1.3 Catalyzed GPF

Figure 4-7 is a compilation plot for pressure drop versus ash load for filters C1 to C4 generated in loading Experiment 3. The transition zone from deep bed filtration to cake filtration described in section 4.1.1 occurs from 2.5-5g/L ash load, which is the equivalent of 2,500 to 5,000 miles road miles sooner than the transition zone for un-catalyzed filters loaded in Experiment 1.

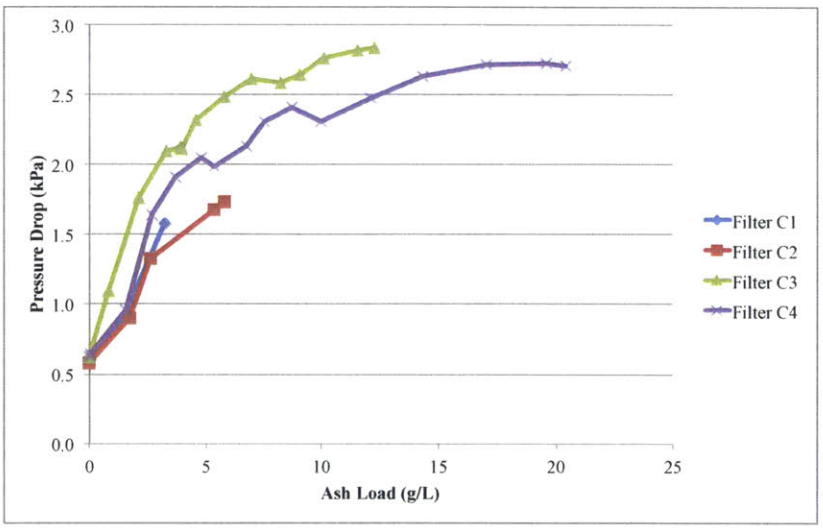

Figure 4-7 – Filter C1 - C4; Pressure Drop vs. Ash Load at Space Velocity 45,000 hr^{-1}

To determine the impact of porosity on the onset of filtration mode transition, the Experiment 3 pressure drop data is normalized to filter subsurface layer void volume in Figure 4-8. The transition zone occurs from 45% to 65% void volume filling for Experiment 3. The transition range for Experiment 3 occurs at higher void filling than the transition range for Experiment 1. The higher void volume filling at the transition point for Experiment 3 versus Experiment 1 indicates that porosity is not a dominant variable in the onset of filtration mode transition for these GPFs. The change in the relative onset of the transition zone between the two experiments is driven by the difference in the normalizing value, the theoretical void volume. This result does indicate that the lower porosity filter is capable of holding higher amounts of ash per unit volume in the porous network of the filter walls, but porosity does not significantly impact the onset of transition as a function of ash load or road miles of GPF age.

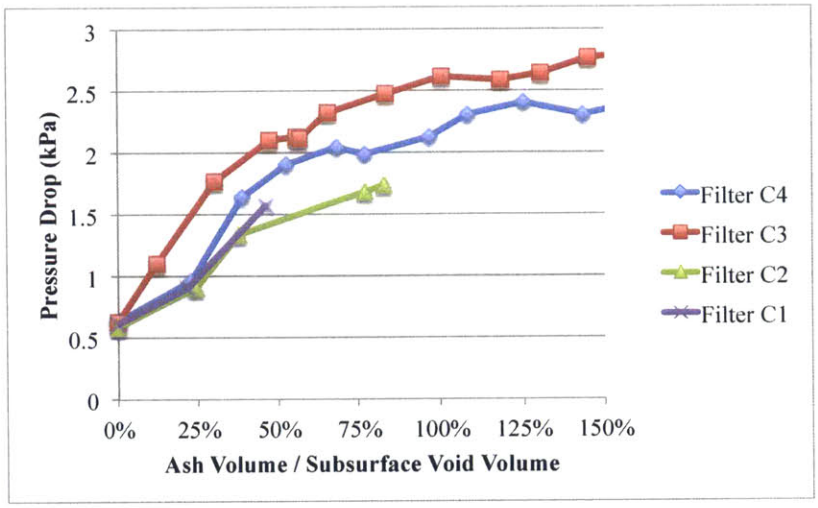

Figure 4-8 - Filters C1 - C4; Pressure Drop vs. % Subsurface Void Volume Filling at Space Velocity 45,000 hr^{-1}

Catalyzed filter pressure drop results do not show a dominant repeatable trend during or after the transition zone. Filters 1 to 5 show a repeatable trend in pressure drop versus ash load with filter 4 deviating from that trend. Filters C1 to C4 show an even spread in pressure drop trends above 3g/L ash when filtration mode transition begins. Larger data sets for all filter types are required to characterize the variance of the pressure drop resulting from ash deposition in the filter, but the available data does suggest that it is more difficult to determine the maximum end of life GPF pressure drop for the lower porosity catalyzed filters tested than for the higher porosity un-catalyzed filters of Experiment 1.

The impact of a catalyst wash coat on ash deposit mechanisms and the associated impact on filter performance is a complex issue that requires further study at the macroscopic and microscopic level. However, current data does indicate that catalyzed filters are more susceptible to ash induced pressure drop. One possible cause of this vulnerability is the effect that wash coat application has on the porous network of the GPF's cordierite channel walls. Alumina wash coat enters the GPF as a liquid. The physical processes that drive the distribution of the wash coat in the filter are different than those that drive the formation of the underlying ceramic substrate. This adds an independent random process to the manufacturing process that may increase variance in the final product's performance. Surface tension may drive the wash coat to collect disproportionally in narrow areas of the cordierite's porous network. Wash coat deposits that

restrict narrow passages within the filter would reduce porous network connectivity and increase the probability that subsequent ash deposits could block narrow passages creating large increases in the flow resistance of the filter. Uneven distribution of wash coat in a C-GPF channel wall favoring collection in narrow passages is shown in Figure 4-9.

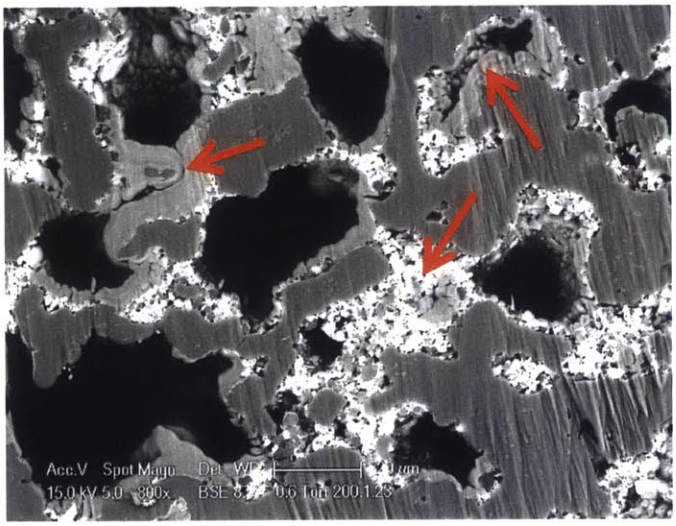

Figure 4-9 – Cross section of a cordierite wall with Alumina wash coat present. Red arrows indicate areas where wash coat is concentrated in narrow regions of the cordierite porous network. Image courtesy of Dr. C.J. Kamp.

4.2 Catalyst Performance for Ash Loaded C-GPFs

The engine cold start portion of the EPA certified test cycle accounts for the majority of pollutant emissions from modern engines. TWC warm-up is one major factor causing increased emissions during cold start [11]. The TWC must warm from ambient temperatures to over 200^{O}C before the chemical reactions responsible for removing HC, CO, and NO_X will commence. The threshold temperature for TWC chemical reactions is referred to as the TWC light-off temperature. The presence of ash has been shown to increase the catalyst light-off temperature for CO oxidation in a DPF by 20^{O}C [28]. NO_X, CO, and HC emissions have been shown to increase linearly with increasing ash deposits in a TWC [35]. To determine the possible ash impacts on C-GPF, temperature ramp experiments were conducted to characterize the light-off temperature in the C-GPF samples generated in Experiment 3.

Each filter sample, including a clean sample free of ash, was tested under lean light-off and near-stoichiometric exhaust conditions. The light-off temperatures for each of the TWC chemical reactions are listed in Table 4-2. Results are plotted in Figures 4-10 and 4-11.

Table 4-2 – Catalyst Light-off Temperatures at Varied Exhaust Conditions, Catalyst Load, and Ash Load

Light-off Temp in Deg C; 10g Catalyst Load						
	Lean			Stoichiometric		
Filter	NO	CO	HC	NO	CO	HC
CC	-	205	235	265	200	260
C2	-	228	280	325	290	330
C4	-	230	280	335	300	345

Light-off Temp in Deg C; 3g Catalyst Load						
	Lean			Stoichiometric		
Filter	NO	CO	HC	NO	CO	HC
C1	-	260	295	380	295	320
C3	-	310	345	410	335	360

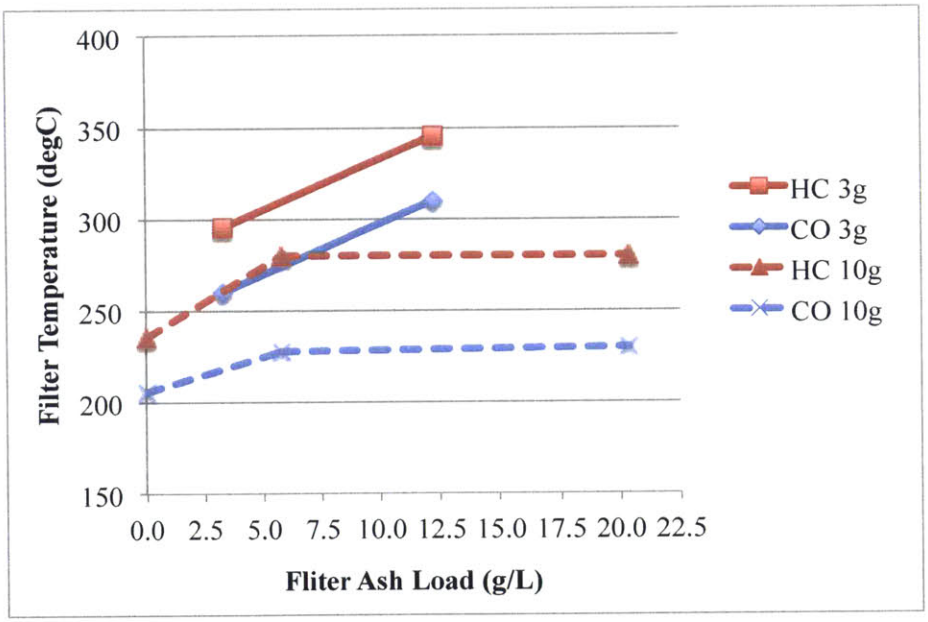

Figure 4-10 – Light-off Temperature versus Ash Load; Lean Exhaust

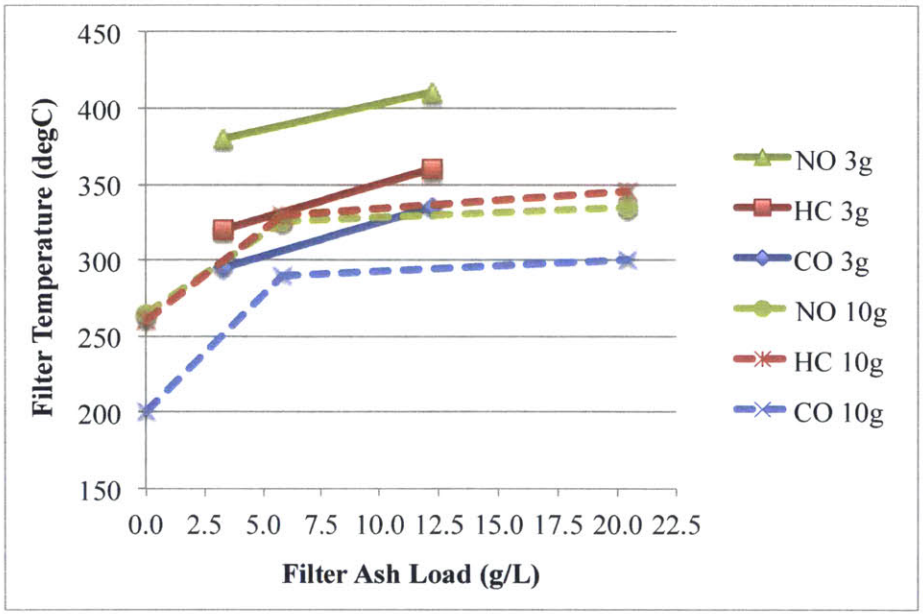

Figure 4-11 – Light-off Temperature versus Ash Load; Near-stoichiometric Exhaust

Results show an increase in light-off temperatures with added ash load regardless of the C-GPF catalyst loading level, specific chemical reaction, and exhaust conditions. Results do show a strong dependence on catalyst loading level. Filter C4 exhibits lower light-off temperatures than filter C3 for all reactions in all exhaust conditions. Filter C4 is loaded to 20g/L ash compared to C3's 12g/L load, but C4 is coated with $10g/ft^3$ catalyst loading compared to C3's $3g/ft^3$.

Filter CC, C2, and C4 demonstrate a non-linear increase in the catalyst light-off temperature with increasing ash load. Over the service life of the GPF from 0g/L to 20g/L of ash load, light-off temperature increase 25-50^{O}C for lean exhaust conditions and 70-100^{O}C for near-stoichiometric exhaust conditions. In all cases more than 80% of the service life increase in light-off temperature occurred between 0g/L and 6g/L of ash load. This is consistent with previous research on catalyzed DPFs that found that all increases in catalyst light-off temperature due to ash deposits can be traced to the early stages of ash accumulation in the filter [28].

Results for the $3g/ft^3$ loading level show an increase in light-off temperature from low (3g/L) to moderate (12g/L) ash levels. Further trends cannot be determined without data for additional ash loads. Future work will include catalytic testing of a clean C-GPF sample with $3g/ft^3$ catalyst

loading to better characterize the increase in catalyst light-off temperature with ash load early in a C-GPF's service life.

4.3 Ash Distribution in Un-catalyzed GPF

Ash distribution for filters 4 and 5 was determined following the procedure described in section 3. Filters 1 through 3 do not exhibit sufficiently thick wall layers for this particular analysis method. The ash layer thickness and the ash plug location relative to longitudinal filter position are shown in Figure 4-12.

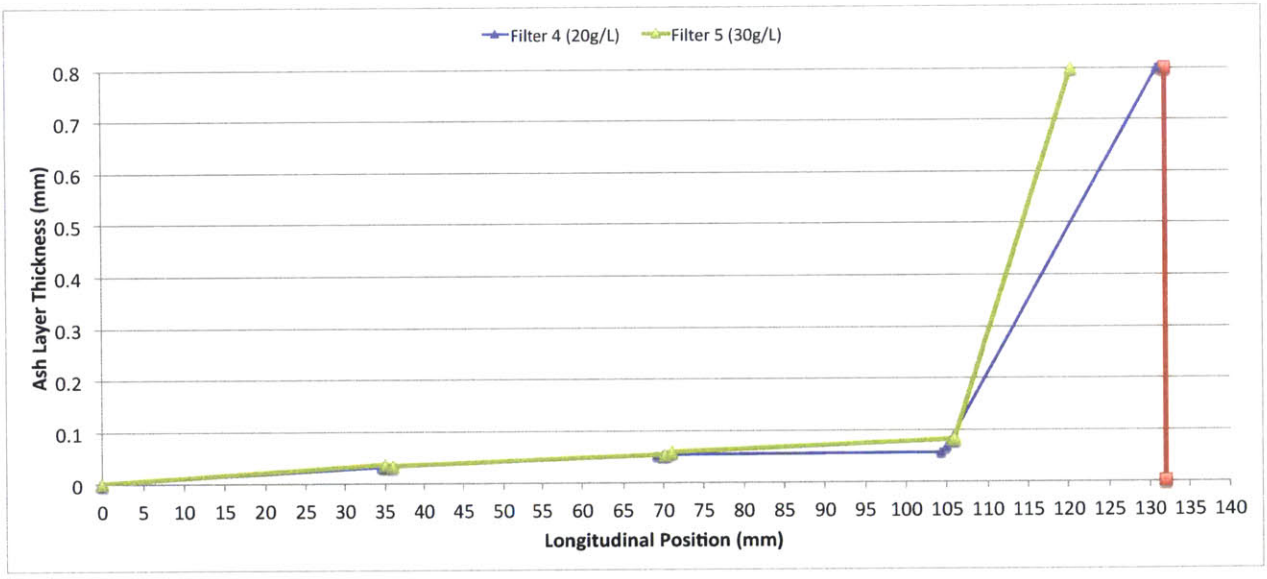

Figure 4-12 – Filters 4 and 5; Ash Wall Layer Thickness and Plug Length

The distribution data for filters 4 and 5 show minimal growth of the wall layer thickness from 20g/L to 30g/L ash loading. No ash plug is evident in filter 4. A 10mm ash plug is present in filter 5. The apparent development of an ash plug without significant increase in the wall layer thickness causes a relatively low increase of 0.4kPa in the pressure drop of filter 5 during the final 30% of its service life. If all of the ash added from 20g/L to 30g/L ash load were deposited on the wall layer, the average increase in layer thickness would be 0.02mm. This 50% increase in the average wall layer thickness would result in a similar increase in pressure drop. The smaller increase in pressure drop observed over this period can be partially attributed to the deposit of a significant mass of ash in the ash plug.

The packing density of the wall layer and ash plug for filters 4 and 5 is derived experimentally using the procedure described in section 3.2. No ash plug packing density can be calculated for filter 4 because no appreciable ash plug is present in the sample. The packing densities are given in Figure 4-13 and compared to some historical DPF data.

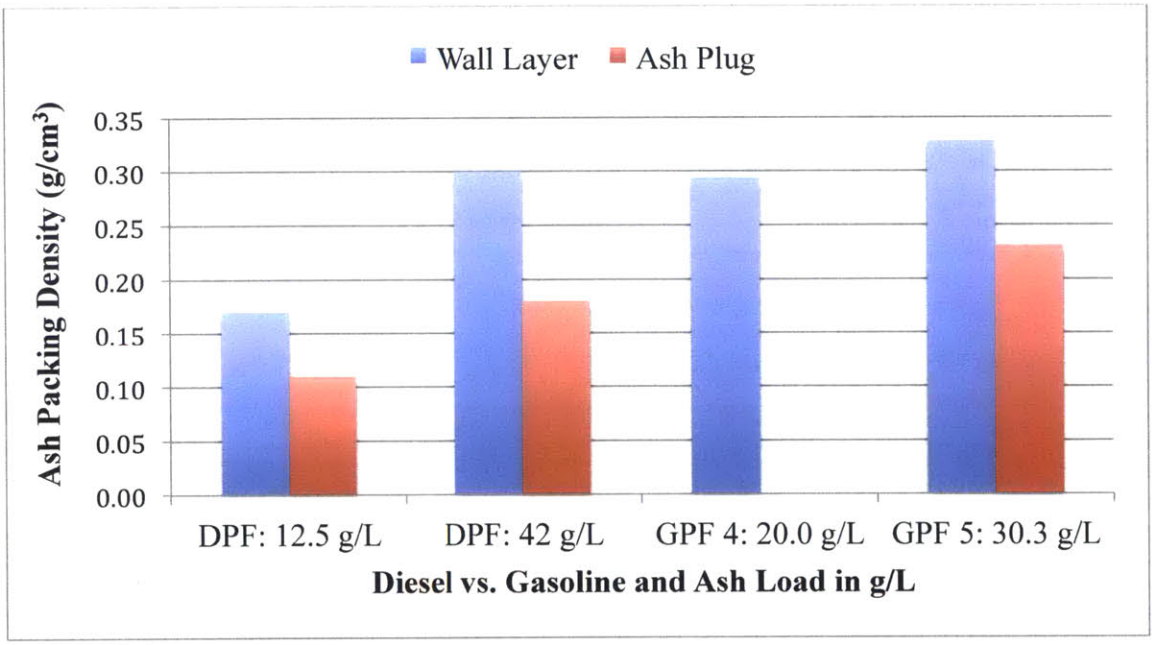

Figure 4-13 – Wall Layer and Ash Plug Packing Densities for Filters 4 & 5 and Historical DPF data [25]

GPF ash packing densities are consistent with historical DPF values. GPFs also demonstrate lower packing densities in the ash plug than the wall layer following the historical DPF trend. Additional GPF samples are required to understand the impact of varied exhaust conditions and GPF configurations on ash deposit packing density. Ash distribution and packing density analysis will be completed for C-GPFs from Experiment 3 as part of ongoing efforts to characterize ash impacts on GPF performance.

5. Conclusions

5.1 GPF Pressure Drop Response to Ash

Ash impacts on GPF pressure drop performance can be divided into three filtration modes that have unique pressure drop response trends. The deep bed filtration regime is characterized by a steep rise in the GPF pressure drop in response to the first 3-5g/L of ash load equivalent to 15,000-25,000 road miles. The slope of pressure drop response during deep bed filtration is an order of magnitude greater than the response slope during cake layer filtration. The cake layer filtration mode occupies 65-75% of the GPF service life but accounts for only 35-45% of the rise in pressure drop during the life of the filter.

The transition from deep bed filtration to cake layer filtration is a critical process that will impact the pressure drop performance of a GPF for the remainder of its service life. A pressure drop increase of 0.5kPa manifested in the transition zone for filter 4 when compared with filters 2, 3, and 5. The 0.5kPa increase persisted for the remainder of filter 4's services life when compared with filter 5. Strategies to accelerate the onset of filtration mode transition in order to minimize the GPF pressure drop when cake filtration begins will result in lower pressure drop with improved engine output and efficiency for the remaining 70% of the system's service life.

5.2 GPF Pressure Drop Response to Soot

Soot impacts on GPF pressure drop performance demonstrate two response modes similar to the response to ash loading. The data available suggests the presence of a deep bed filtration regime but sufficient data is not available to full characterize the resulting pressure drop response. Experiments show that the soot cake filtration regime results in a linear pressure drop response with a consistent slope across the majority of the filter service life.

Cake filtration is the sole soot filtration mode after the onset of ash cake layer formation. This is supported by experiments that show a linear response to soot loading with consistent slope and y-intercept not significantly different from zero for ash load levels from 5g/L to 25g/L. The consistent linear response is significant for engine control schemes because it simplifies

determination of real-time filter soot load based on pressure drop feedback that can easily be provided by onboard sensors.

Formation of an ash cake layer in the GPF tested does not offer a net reduction in soot loaded pressure drop. Previous DPF research suggested that an ash membrane effect preventing entry of soot into the porous network of the filter wall could reduce the soot loaded pressure drop for an ash loaded filter compared to a filter with no ash. This effect was not present in this experiment because the deep bed filtration of soot in the clean filter did not cause a significant enough increase in pressure drop. The possible benefit is derived from eliminating the pressure drop due to soot deep bed filtration and in this case, removing that filtration mode did not eliminate a major contributor to the overall GPF pressure drop performance.

5.3 Ash Impacts on Catalytic Activity in C-GPF

Ash deposits do mask the catalyst particles in the C-GPF preventing reactants in the exhaust stream from reaching active sights. The presence of ash deposits increases the light-off temperature of all three chemical reactions promoted by the TWC coating. Light-off temperatures can increase as much as $100^{O}C$ during the service life of a C-GPF. Higher catalyst loading levels in the C-GPF do result in lower light-off temperatures for all reactions; but $25^{O}C$ to $100^{O}C$ increases in light-off temperature were observed for the $10g/ft^3$ loaded C-GPFs, which constitutes a significant reduction in catalyst performance. A large majority (80-90%) of the increase in catalyst light-off temperature occurred in the first 20% of the C-GPF's service life reducing the catalyst performance for the remaining 80% of its service life in the vehicle.

The increases in light-off temperature demonstrated by this study will greatly inhibit the system's ability to limit cold start emissions to meet regulatory limits. Reductions in catalytic activity due to C-GPF ash loading are an important variable impacting design of an exhaust treatment system employing a TWC and C-GPF in tandem. The impact of ash on C-GPF catalytic performance, particularly during cold start, must be fully understood before implementation of a notional "four-way catalyst" relying solely on a C-GPF for NO_X, CO, and HC as discussed in [24].

6. Future Work

The accelerated ash loading system is a powerful tool that allows for systematic study of all the variables that impact the performance of GPFs. The full potential of this tool will not be realized until a large number of samples have been generated across a wide range of GPF configurations and exhaust conditions representing varied engine operating schemes. Detailed analysis of a large GPF sample library using advanced diagnostic tools will continue to uncover important principles governing the formation of ash deposits in GPFs and the impact of those deposits on pressure drop performance.

Control over the AFR of the simulated exhaust stream generated by the accelerated aging system must be improved in order to simulate (and experiment with variations to) the coast and deceleration regeneration strategy discussed in 1.3.8.2. To fully simulate the oxygen pulse regeneration strategy the system must be upgraded with an automated feedback loop capable of varying the system flow rate to maintain a target AFR and capable of varying the AFR on a time scale of seconds or tens of seconds. With this capability the impact of different regeneration strategies on ash deposits and ash related pressure drop could be studied within the narrow envelope of possible GPF regeneration methods.

Improved control of AFR in the catalyst flow bench could also provide additional insight into C-GPF performance. The current flow bench does not include an oxygen modulation capability. This capability would mimic AFR modulation in an engine to deliver a simulated exhaust stream with varying oxygen content. A properly modulated inlet stream will engage the oxygen storage catalyst present in C-GPF improving the accuracy of catalytic activity tests and furthering our understanding of the impact of ash on catalyst performance.

Additional GPF samples generated on the accelerated aging system will be analyzed using the ash distribution analysis technique discussed in section 3. Changes in ash distribution and packing density due to changes in GPF configuration and exhaust conditions could be correlated to differences in measured pressure drop performance. Ash distribution and packing density data can also be applied to classical filtration models to predict the impact of certain experimental variables on filter performance to aid in the design and implementation of GPFs in the future.

(This Page Intentionally Left Blank)

References

[1] United States Energy Information Administration. "Energy Explained." *EIA.gov*. U.S. Energy Information Administration, 2015. Web. 20 Apr. 2015. <http://www.eia.gov/energyexplained/>.

[2] United States Environmental Protection Agency. "Sources of Greenhouse Gas Emissions." *EPA.gov*. U.S. Environmental Protection Agency, 2015. Web. 20 Apr. 2015. <http://www.epa.gov/climatechange/ghgemissions/sources.html>

[3] United States Environmental Protection Agency. "EPA and NHTSA Finalize Historic National Program to Reduce Greenhouse Gases and Improve Fuel Economy for Cars and Trucks." *EPA.gov*. U.S. Environmental Protection Agency, 2010 Apr. Web. 20 Apr. 2015. <http://www.epa.gov/otaq/climate/regulations/420f10014.pdf>

[4] United States Environmental Protection Agency. "EPA and NHTSA Set Standards to Reduce Greenhouse Gases and Improve Fuel Economy for Model Years 2017-2025 Cars and Light Trucks." *EPA.gov*. U.S. Environmental Protection Agency, 2012 Aug. Web. 20 Apr. 2015 <http://www.epa.gov/otaq/climate/documents/420f12051.pdf>

[5] United States Environmental Protection Agency. "EPA Sets Tier 3Tailpipe and Evaporative Emission and Vehicle Fuel Standards." *EPA.gov*. U.S. Environmental Protection Agency, 2014 Mar. Web. 20 Apr. 2015 <http://www.epa.gov/otaq/documents/tier3/420f14008.pdf>

[6] European Commission. "COMMISSION REGULATION (EU) No 459/2012 of 29 May 2012 Amending Regulation (EC) No 715/2007 of the European Parliament and of the Council and Commission Regulation (EC) No 692/2008 as Regards Emissions from Light Passenger and Commercial Vehicles (Euro 6)." 29 May 2012. Web. 20 Apr. 2015. <http://eur-lex.europa.eu/legal-content/EN/TXT/PDF/?uri=CELEX:32012R0459&qid=1430082013501&from=EN>.

[7] Kirchner, U., Vogt, R., and Maricq, M., "Investigation of EURO-5/6 Level Particle Number Emissions of European Diesel Light Duty Vehicles," SAE Technical Paper 2010-01-0789, SAE International, 2010. doi:10.4271/2010-01-0789.

[8] Steimle, F., Kulzer, A., Richter, H., Schwarzenthal, D. et al., "Systematic Analysis and Particle Emission Reduction of Homogeneous Direct Injection SI Engines," SAE Technical Paper 2013-01-0248, SAE International, 2013. doi:10.4271/2013-01-0248.

[9] United States Environmental Protection Agency, "2017 and Later Model Year Light-Duty Vehicle Greenhouse Gas Emissions and Corporate Average Fuel Economy Standards" 40 CFR Parts 85, 86, and 600 [Docket [EPA–HQ–OAR–2010–0799; FRL–9706–5; NHTSA–2010–0131]. *GPO.gov*. U.S. Government Publishing Office, 2012 Oct. 15. Web. 20 Apr. 2015. <http://www.gpo.gov/fdsys/pkg/FR-2012-10-15/pdf/2012-21972.pdf>

[10] Heywood, John B. *Internal Combustion Engine Fundamentals*. New York: McGraw-Hill, 1988. Print.

[11] Basshuysen, Richard. *Internal Combustion Engine Handbook Basics, Components, Systems, and Perspectives*. Warrendale, Pa.: SAE International, 2004. Print.

[12] U.S. EPA. "Integrated Science Assessment of Ozone and Related Photochemical Oxidants (Final Report)." U.S. Environmental Protection Agency, Washington, DC, EPA/600/R-10/076F, 2013.

[13] U.S. EPA. "Integrated Science Assessment for Oxides of Nitrogen – Health Criteria (Final Report, 2008)." U.S. Environmental Protection Agency, Washington, DC, EPA/600/R-08/071, 2008.

[14] Drake, M., Fansler, T., Solomon, A., and Szekely, G., "Piston Fuel Films as a Source of Smoke and Hydrocarbon Emissions from a Wall-Controlled Spark-Ignited Direct-Injection Engine," SAE Technical Paper 2003-01-0547, SAE International, 2003, doi:10.4271/2003-01-0547.

[15] U.S. EPA. "Integrated Science Assessment for Carbon Monoxide (Final Report)." U.S. Environmental Protection Agency, Washington, DC, EPA/600/R-09/019F, 2010.

[16] Piock, W., Hoffmann, G., Berndorfer, A., Salemi, P. et al., "Strategies Towards Meeting Future Particulate Matter Emission Requirements in Homogeneous Gasoline Direct Injection Engines," *SAE Int. J. Engines* 4(1):1455-1468, 2011, doi:10.4271/2011-01-1212.

[17] U.S. EPA. "Integrated Science Assessment for Particulate Matter (Final Report)." U.S. Environmental Protection Agency, Washington, DC, EPA/600/R-08/139F, 2009.

[18] Hung, D., Zhu, G., Winkelman, J., Stuecken, T. et al., "A High Speed Flow Visualization Study of Fuel Spray Pattern Effect on Mixture Formation in a Low Pressure Direct Injection Gasoline Engine," SAE Technical Paper 2007-01-1411, SAE International, 2007, doi:10.4271/2007-01-1411.

[19] "Ceramic Catalyst Substrates." *DieselNet Technology Guide*. Ecopoint Inc, 2011. Web. 20 Apr. 2015. <http://www.dieselnet.com.libproxy.mit.edu/tech/cat_subs_cer.php>.

[20] Majewski, W. A. "Diesel Particulate Filters." *DieselNet Technology Guide*. Ecopoint Inc, 2011. Web. 20 Apr. 2015. <http://www.dieselnet.com.libproxy.mit.edu/tech/dpf.php>.

[21] Sappok, Alexander. "The Nature of Lubricant-derived Ash-related Emissions and their Impact on Diesel Aftertreatment System Performance." Massachusetts Institute of Technology, 16 Jun. 2009. Web. 20 Apr. 2015. <http://hdl.handle.net/1721.1/50586>.

[22] Majewski, W. A. "Wall Flow Monolith." *DieselNet Technology Guide*. Ecopoint Inc, 2005. Web. 20 Apr. 2015. <http://www.dieselnet.com.libproxy.mit.edu/tech/dpf_wall-flow.php>.

[23] Majewski, W. A. "Diesel Filter Regeneration." *DieselNet Technology Guide*. Ecopoint Inc, 2005. Web. 20 Apr. 2015. < http://www.dieselnet.com.libproxy.mit.edu/tech/dpf_regen.php>.

[24] Johnson, T., "Review of Vehicular Emissions Trends," *SAE Int. J. Engines* 8(3):2015, doi:10.4271/2015-01-0993.

[25] Sappok, A. G. "Ash Accumulation in Diesel Particulate Filters." *DieselNet Technology Guide*. Ecopoint Inc, 2013. Web. 20 Apr. 2015. <http://www.dieselnet.com.libproxy.mit.edu/tech/dpf_ash.php#properties>.

[26] Nicolin, P., Rose, D., Kunath, F., and Boger, T., "Modeling of the Soot Oxidation in Gasoline Particulate Filters," *SAE Int. J. Engines* 8(3):2015, doi:10.4271/2015-01-1048.

[27] Ito, Y., Shimoda, T., Aoki, T., Yuuki, K. et al., "Next Generation of Ceramic Wall Flow Gasoline Particulate Filter with Integrated Three Way Catalyst," SAE Technical Paper 2015-01-1073, SAE International, 2015, doi:10.4271/2015-01-1073.

[28] Murray, Timothy. "The Effect of Lubricant Derived Ash on the Catalytic Activity of Diesel Particulate Filters." Massachusetts Institute of Technology, 15 Aug. 2014. Web. 20 Apr. 2015. <http://hdl.handle.net/1721.1/92182>.

[29] Bardasz, E., Mackney, D., Britton, N., Kleinschek, G. et al., "Investigations of the Interactions between Lubricant-derived Species and Aftertreatment Systems on a State-of-the-Art Heavy Duty Diesel Engine," SAE Technical Paper 2003-01-1963, SAE International, 2003, doi:10.4271/2003-01-1963.

[30] Sutton, M., Britton, N., Otterholm, B., Tengström, P. et al., "Investigations into Lubricant Blocking of Diesel Particulate Filters," SAE Technical Paper 2004-01-3013, SAE International, 2004, doi:10.4271/2004-01-3013.

[31] Sappok, A., Beauboeuf, D., and Wong, V., "A Novel Accelerated Aging System to Study Lubricant Additive Effects on Diesel Aftertreatment System Degradation," *SAE Int. J. Fuels Lubr.* 1(1):813-827, 2009, doi:10.4271/2008-01-1549.

[32] Jorgensen, James, Timothy Murray, Alexander Sappok, Victor Wong, Christoph Borensen, Christine Lambert, James Pakko, and James Warner. "The Effect of Ash Accumulation on Gasoline Particulate Filters: A Comparison Between Laboratory and Field Aged Samples." *ASME 2014 Internal Combustion Engine Division Fall Technical Conference* 1 (2014). Web. 20 Apr. 2015. <http://proceedings.asmedigitalcollection.asme.org.libproxy.mit.edu/proceeding.aspx?articleid=2022896&resultClick=1>.

[33] Bodek, K. and Wong, V., "The Effects of Sulfated Ash, Phosphorus and Sulfur on Diesel Aftertreatment Systems - A Review," SAE Technical Paper 2007-01-1922, SAE International, 2007, doi:10.4271/2007-01-1922.

[34] Ishizawa, T., Yamane, H., Satoh, H., Sekiguchi, K. et al., "Investigation into Ash Loading and Its Relationship to DPF Regeneration Method," *SAE Int. J. Commer. Veh.* 2(2):164-175, 2010, doi:10.4271/2009-01-2882.

[35] Franz, J., Schmidt, J., Schoen, C., Harperscheid, M. et al., "Deactivation of TWC as a Function of Oil Ash Accumulation - A Parameter Study," SAE Technical Paper 2005-01-1097, SAE International, 2005, doi:10.4271/2005-01-1097.

[36] Gaiser, G. and Mucha, P., "Prediction of Pressure Drop in Diesel Particulate Filters Considering Ash Deposit and Partial Regenerations," SAE Technical Paper 2004-01-0158, SAE International, 2004, doi:10.4271/2004-01-0158.

[37] Dimou, I., Sappok, A., Wong, V., Fujii, S. et al., "Influence of Material Properties and Pore Design Parameters on Non-Catalyzed Diesel Particulate Filter Performance with Ash Accumulation," SAE Technical Paper 2012-01-1728, SAE International, 2012, doi:10.4271/2012-01-1728.